Causes for the increases in both evapotranspiration and water yield over vegetated mainland China during the last two decades

Shanlei Sun [a,*], Yibo Liu [b], Haishan Chen [a], Weimin Ju [c], Chong-Yu Xu [d], Yi Liu [e], Botao Zhou [a], Yang Zhou [a], Yanlian Zhou [f], Miao Yu [a]

[a] Collaborative Innovation Center on Forecast and Evaluation of Meteorological Disasters/Key Laboratory of Meteorological Disaster, Ministry of Education/International Joint Research Laboratory on Climate and Environment Change, Nanjing University of Information Science and Technology, Nanjing, China
[b] Jiangsu Key Laboratory of Agricultural Meteorology, School of Applied Meteorology, Nanjing University of Information Science and Technology, Nanjing, China
[c] International Institute for Earth System Science, Nanjing University, Nanjing, China
[d] Department of Geosciences, University of Oslo, Oslo, Norway
[e] School of Civil and Environmental Engineering, The University of New South Wales, Sydney, Australia
[f] School of Geographic and Oceanographic Sciences, Nanjing University, Nanjing, China

A R T I C L E   I N F O

A B S T R A C T

Quantifying the contributions of climate and vegetation to the dynamics of evapotranspiration (ET) and water yield (i.e., precipitation minus ET) will help us better understand the changes in the water budget. In this study, we identified the contributions of climate variables (including precipitation, radiation, temperature, and relative humidity), human-disturbed vegetation, and natural vegetation to the trends in annual ET and water yield over vegetated mainland China during 2001–2020, using a process-based terrestrial ecosystem model and a joint-solution method with multiple sensitivity numerical experiments. Results showed that 46% of the study area experienced significant ($p<0.05$) increases in ET, with an overall increase of 2.32 mm y^{-1}. Meanwhile, the overall trend in water yield was 2.56 mm y^{-1} but insignificant. Spatially, vegetation and precipitation are the dominant factors for ET trends over 55% and 32% of vegetated mainland China, respectively. Over the regions where vegetation dominates the ET trends, nearly half of these regions are covered by human-disturbed vegetation (e.g., cropland or regions with land cover changes), suggesting that anthropogenic activities play a crucial role in the hydrological cycle there. Concerning the trends in water yield, precipitation is the dominant factor over 64% areas. Human-disturbed vegetation and natural vegetation play similar roles and combined can explain the water yield trends over 30% areas. Our study highlights the spatial variations in the mechanisms behind changes in the water budget over mainland China, particularly in regions covered by human-disturbed vegetation. This finding should be considered in the existing and future national ecological recovery policies to maximize its eco-hydrological benefits.

1. Introduction

Evapotranspiration (ET) is arguably a central component of the terrestrial water cycle, and functions as a vital link between the land surface and the atmosphere through water, energy, and carbon cycles, thereby having important implications for the availability and usage of water resources (Seneviratne et al., 2006; Wang and Dickinson, 2012). Therefore, the spatio-temporal pattern of ET changes has always been a common concern of the scientific community, and has been intensively studied from global to regional scales (Potter et al., 2005; Fernandes et al., 2009; Marshall et al., 2012; Williams et al., 2012; Sun et al., 2014, 2021; Teuling et al., 2019; Bai et al., 2020; Zhang et al., 2020; Li and Quiring, 2021; Ruscica et al., 2021). In a word, the changes in ET have happened on various spatio-temporal scales during the past several decades but are mainly characterized by evident spatial differences. However, our knowledge of the main factors controlling changes in ET and even the relevant physical mechanisms are still insufficient, which are the key basis for science-based management and rational allocation of water resources (Milly et al., 2005; Ribes et al., 2013).

To that end, the mechanisms behind the changed ET have been extensively elucidated by a wealth of studies from perspectives of climate conditions and land surface properties (Williams et al., 2012;

---

* Corresponding author.
E-mail address: sun.s@nuist.edu.cn (S. Sun).

Odongo et al., 2019; Sun et al., 2014, 2021; Zhang et al., 2018, 2020). Studies suggested that changes in climate conditions (e.g., global warming and dimming/brightening, wind stilling, and changes in precipitation and relative humidity/vapor pressure deficit) dominated the variations of ET in some regions through regulating water and energy conditions. In contrast, other regions exhibited dominant factors of land surface properties. Among the land surface properties, vegetation has multiple biophysical properties. This is especially true for the key biophysical parameter of the leaf area index (LAI), which is most often used to describe vegetation dynamics and largely determines the allocation of available water and energy (Katul et al., 2012; Zhang et al., 2018; Cavalcante et al., 2019). Moreover, vegetation is also the most ever-changing due to plant growth, natural disturbances, and anthropogenic disturbances (Liu et al., 2016a, 2016b; Papagiannopoulou et al., 2017; Cavalcante et al., 2019; Zhang et al., 2020). Therefore, these dictate that the impacts of vegetation on changes in ET and other water cycle components are complex (Katul et al., 2012; Ruiz-Pérez et al., 2016). For example, it is widely believed that forestation and deforestation have the functions of increasing and declining ET, respectively (Sun et al., 2006a; Yang et al., 2009; Feng et al., 2016, 2021b; Cavalcante et al., 2019; Xie et al., 2020). By contrast, forestation and deforestation's effects on water yield or runoff are still disputed up to now (Ellison et al., 2012). Some studies found that forestation could reduce water yield or runoff, generally through increasing evaporation of canopy interception, transpiration, and at last, ET (Brown et al., 2005; Cavalcante et al., 2019). Conversely, other studies have shown that forestation increases water yield or runoff because forestation can lead to increased precipitation (larger than the increases in forestation-induced ET) on regional to global scales via facilitating large-scale transport of water vapor, which is known as the climatic effect of forestation (Pielke, 2005; Sheil and Murdiyarso, 2009; Yosef et al., 2018). To sum up, vegetation-induced hydrological effects remain controversial, mainly due to the complexity of vegetation dynamics and multiway interactions and feedbacks among vegetation, atmosphere and hydrology.

Although large areas of forests are destroyed annually due to anthropogenic and natural disturbances across the globe, the Earth's lands are becoming greening, which has been consistently evidenced by different satellite vegetation indicators (including LAI; Jong et al., 2012; Mao et al., 2013; Zhu et al., 2016; Chen et al., 2019a; Cortés et al., 2021). In particular, China, with only 6.6% of the global vegetated area alone, accounts for 25% of the global net increase in leaf area index (LAI) during 2000–2017 (Chen et al., 2019a). Two major factors, including direct factors (e.g., human disturbances, such as afforestation/reforestation, and croplands abandonment) and indirect factors (e.g., plant growth under the natural environmental conditions, such as CO_2 fertilization and nitrogen deposition), should be responsible for China's greening (Xiao, 2014; Chen et al., 2015, 2019a). For mitigating land degradation, air pollution, and climate change, the Chinese government has implemented a series of nationwide ecosystem restoration programs since the late 1980s, such as the "Three-North Forest Shelterbelt Program", the "Natural Forest Conservation Program", and the "Grain for Green Program", and planted millions of trees, consequently increasing vegetation coverage over China (Cao et al., 2011; Chen et al., 2019a). It is believed that China is the country with the largest planted forest area over the world (Liu et al., 2016a, 2016b). Meanwhile, with the fast urbanization in China due to the rapid economic development, more and more people have migrated to cities in recent years, and thereby vast tracts of croplands are abandoned (Qu et al., 2018; Feng et al., 2021a). Besides, the indirect factors can also play a non-negligible role in China's increased greenness and even a comparable role in some regions (e.g., Tibetan Plateau) relative to human disturbances (e.g., Mao et al. 2013; Zhong et al. 2019).

The apparent vegetation greening and climate change across China during the past decades provide a good research opportunity to examine the hydrological responses to changes in vegetation and climate. To date, based on different models and mathematic methods, many studies have been conducted to quantify the impacts of changes in vegetation and climate on ET, runoff and other hydrological variables at various spatio-temporal scales (Liu et al., 2015a, 2016a, 2016b; Bai et al., 2020; Lian et al., 2020; Zhang et al., 2018, 2020; Xie et al., 2019, 2020; Feng et al., 2021b). Briefly, vegetation greening could result in increase (decrease) in annual ET (water yield or runoff) and the transpiration ratio to ET. However, it should be noted that the vegetation greening-induced changes in the hydrological variables varied noticeably in space. These previous studies provide important references for scientifically understanding the role of vegetation greening in the changed hydrological processes across China. However, several major limitations should be noted. Firstly, due to no considerations of the impacts of interactions among the influential factors, there often exist uncertainties and even errors for the contributions estimated by the traditional separation methods, such as regression analysis (Xie et al., 2020), sensitivity method (Sun et al., 2013; Zhang et al., 2020), differential equation approach (Yang et al., 2009, 2014; Zhang et al., 2018), and traditional numerical experiment approach (comparing the simulations under different scenario settings; e.g., Liu et al., 2016b; Bai et al. 2020; Zhang et al., 2020). Considering this issue, Sun et al. (2014, 2017, 2021) developed a joint-solution method with multiple sensitivity numerical experiments. This method can eliminate the combined effects of the influential factors' interactions, and provides an efficient tool for accurately estimating the contributions of each factor to changes in the hydrological variables. Secondly, only a few studies have separated the contributions of human-disturbed and natural vegetation to the variations of key hydrological variables across China, and identified the dominant factor among climate variables, human-disturbed vegetation and natural vegetation. Therefore, further studies are still needed to dig into vegetation's role in the changes of hydrological processes from the perspectives of impacts of human-disturbed vegetation and natural vegetation.

In this study, the Boreal Ecosystem Productivity Simulator (BEPS) model will be used to simulate ET, mainly because of its superiority and successful applications in estimating terrestrial carbon and water fluxes in various ecosystems in different regions (Amthor et al., 2001; Matsushita and Tamura, 2002; Wang et al., 2004; Ju et al., 2006, 2010a, 2010b; Schwalm et al., 2010; Liu et al., 2015b, 2016b; Sonnentag et al., 2008; Sprintsin et al., 2012; Luo et al., 2018; Chen et al., 2019b; He et al., 2021). Importantly, its simulation capability has been enhanced in China's terrestrial ecosystems through optimizing parameters based on the literatures (e.g., Feng et al., 2007; Zhang et al., 2012) and eddy covariance (EC) flux tower observations (e.g., Liu et al. 2015b, 2016b). Therefore, we will proceed with this study using the BEPS model and the joint-solution method with multiple sensitivity numerical experiments. The objective of this study is twofold. First is to investigate the trends in ET, water yield (i.e., precipitation minus ET), climate variables (including precipitation, radiation, temperature, and relative humidity), and vegetation (including human-disturbed and natural vegetation) over mainland China during 2001–2020. Second is to quantify the contributions of climate variables and vegetation dynamics to the trends in ET and water yield using the joint-solution method (details in Section 2.4; Sun et al., 2017) and consequently determine the major driving factors of the ET and water yield trends during the last two decades over different regions (i.e., ten first-level water resources regions; Fig. 1a). The results based on the new separation method can provide quantitative information to better understand the underlying mechanisms of hydrological processes across China and scientifically maintain water resources' sustainable utilization. Importantly, distinguishing the contributions of human-disturbed vegetation and natural vegetation will help science-based ecosystem restoration planning.
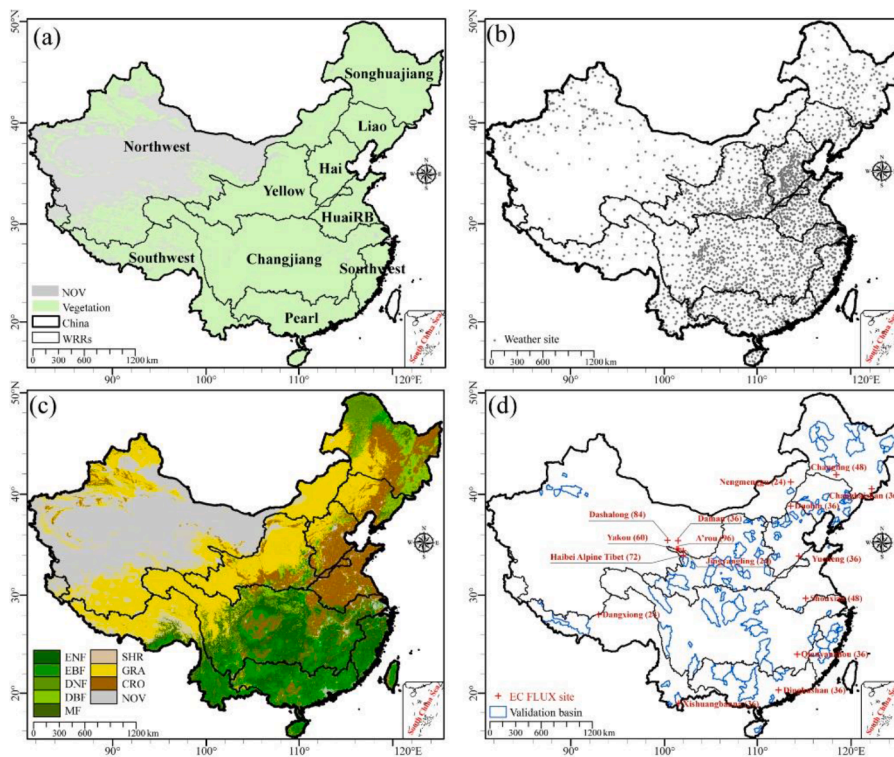
Fig. 1. Spatial distributions of ten first-level water resources regions, weather sites, MODIS-based land use/cover (LC) in 2001, and eddy covariance (EC) flux sites and validation basins used to evaluate water-balance simulations. (a) Spatial distribution of ten first-level water resources regions. Water resources regions include Songhuajiang, Liao, Northwest, Yellow, Hai, Huai, Changjiang, Southeast, Southwest, and Pearl River Basin (RB). (b) Spatial distribution of weather sites. (c) Spatial distribution of MODIS-based land use/cover (LC) in 2001 according to the IGBP classification scheme (Liu et al., 2015b). ENF is for evergreen needleleaf forests, EBF for evergreen broadleaf forests, DNF for deciduous needleleaf forests, DBF for deciduous broadleaf forests, MF for mixed forests, SHR for shrublands, GRA for grasslands, CRO for croplands, and NOV for non-vegetation (including urban, barren, permanent snow and ice, and water bodies). (d) Spatial distribution of 16 EC flux sites and 127 validation basins used to evaluate water-balance simulations. The numbers in the brackets represent the monthly data samples of the EC observations, e.g., 36 representing 36 monthly data points.

2. Data and methodology

2.1. The BEPS model

The present study estimated ET on a daily scale using the BEPS model. It was originally proposed based on the frames of the FOREST Bio-Geochemical Cycles (FOREST-BGC) model (Running and Coughlan, 1988), and subsequently improved by several follow-on studies (Chen et al., 1999; Liu et al., 2003; Ju et al., 2010a, 2010b). This model generally includes four components: photosynthesis, energy balance, hydrological, and soil biochemical modules. Within the hydrological module, both transpiration and evaporation are estimated based on the Penman-Monteith equation. ET is computed as the sum of canopy transpiration from sunlit and shaded leaves, canopy interception, and soil surface evaporation (details in *Appendix A*; Chen et al., 2005). The BEPS employs a bucket model approach to simulate soil water content at three soil profile layers with thicknesses of 0.1 m, 0.25 m, and 0.85 m (details in *Appendix B*; Liu et al., 2013).

Following previous studies, we assumed no anthropogenic water use interventions (e.g., the farmland irrigation, the ground water withdrawal, and the inter-basin water transfer projects), and specified water yield as precipitation minus ET, which represents the total amount of water available for runoff, soil water storage change, groundwater recharge, and cryospheric water storage change (if glaciers existed) (Seager et al., 2013; Kumar et al., 2014; Byrne and O'Gorman, 2015). This indicator has been widely used as an informative indicator of water resource conditions to reveal the spatio-temporal changes in water resources across the globe (e.g., Seager et al. 2013, Kumar et al. 2014, Byrne and O'Gorman 2015, Greve and Seneviratne 2015, Greve et al. 2018, Rohatyn et al. 2018, Zhou et al. 2021, Zhao et al. 2021).

Considering the applicability of the BEPS model and the major focuses of this study to investigate climate and vegetation impacts on ET and water yield trends, the simulations were conducted only in the vegetated regions, which were specified as regions always covered by vegetation during 2001–2020. Then, all the area percentages mentioned in the following text were estimated relative to the vegetated regions.

2.2. Data and processing

2.2.1. Inputs for the BEPS model

Routine meteorological observations, land surface parameters [e.g., soil texture, land use/cover (LC), and LAI], and atmospheric CO_2 concentration are necessary to run the BEPS model. Therefore, we collected daily meteorological observations at more than 2000 sites during 2001–2020 from the China Meteorological Administration (CMA; Fig. 1b), i.e., maximum and minimum temperatures (° C), relative humidity (%), sunshine duration (h day^{-1}), and precipitation (mm), which have been performed a strict quality control by the CMA. Furthermore, due to limited spatial representativeness of incoming solar radiation measurements across China (less than 150 sites with observations), the daily sunshine duration was employed to estimate incoming solar radiation following the work of Ju et al. (2010a, 2010b). For matching the spatial resolution (i.e., 500 m) of remotely sensed data (i.e., LC and LAI), the daily meteorological observations were interpolated to 500 m × 500 m gridded data with the inverse distance weight (IDW) interpolation method. Especially for temperature interpolation, the topographic effects (i.e., a lapse rate of 0.6 °C per 100 m) were considered (Liu et al., 2015b).

The volumetric percentages of sand, clay, and silt were from the soil texture maps (http://globalchange.bnu.edu.cn/), which were developed by Shangguan et al. (2012) based on the 1: 1,000,000 scale soil map of China and approximately 9000 soil profile records in the second national soil survey dataset. Each volumetric percentage was resampled at a spatial resolution of 500 m. These percentage data were used to determine hydraulic parameters.

The 2001–2019 annual Moderate Resolution Imaging Spectroradiometer (MODIS) LC products (i.e., MCD12Q1 V006 at a spatial resolution of 500 m; Friedl et al., 2010; Sulla-Menashe et al., 2019) with the International Geosphere-Biosphere Programme (IGBP) land cover classification system were used here (https://lpdaac.usgs.gov/products/mcd12q1v006/), and further aggregated into nine types to assign LC classifications within the BEPS model (details in Fig. 1c). Due to the 2020 dataset deficiency, the corresponding LC map was specified by the

2019 product. This was mainly based on the assumption of small differences in LC types between the adjacent two years, which might have limited impacts on our results.

To represent vegetation characteristics within the BEPS, we collected the 8-day and 500 m GLOBMAP V3.0 LAI product (http://modis.cn/globalLAI/) from 2001 to 2020 (Liu et al., 2012). Effective LAI was produced with the inversion algorithm of the 4-Scale geometric optical model (Deng et al., 2006) using cloud masked MODIS collection 6 land surface reflectance data (MOD09A1; Liu and Liu, 2013), and then converted to true LAI using the 500 m global clumping index data (He et al., 2012). Moreover, a locally adjusted cubic-spline capping approach (LACC; Chen et al., 2006) was applied to remove the unrealistic fluctuations of the LAI induced by residual cloud contamination and atmospheric noises. Some studies have proved that this LAI dataset was superior to others and extensively used globally (Piao et al., 2015; Chen et al., 2019b; Yuan et al., 2019).

2.2.2. Data for validating the BEPS model

For validating the BEPS model performances according to magnitudes of ET and water yield, observed streamflow and EC-based ET measurements were collected in this study. Here, considering the BEPS model simulations only for the vegetated regions, 127 validation basins were chosen following the criterion that the area percentage with non-vegetation (abbreviated as NOV) for each basin should be less than 5%. The annual streamflow records of the 127 basins during 2001–2010 were obtained from the Hydrological Yearbook issued by the Hydrological Bureau of the Ministry of Water Resources of China. These validation basins were distributed across diverse climate regimes and landscape conditions (Fig. 1d), with drainage areas from 186 km^2 to 5,8204 km^2. Multi-year mean annual ET of each basin was calculated as differences between multi-year means of precipitation and streamflow based on the water balance concept, and further used to evaluate the BEPS performances from the climatological perspective. Of the selected 16 eddy covariance (EC) flux sites (Fig. 1d), three, seven, one, and five are from ChinaFlux (http://www.chinaflux.org/; Wen et al., 2005; Fu et al., 2006; Guan et al., 2006; Li et al., 2006; Sun et al., 2006b; Zhang et al., 2006a, 2006b; Chen et al., 2009), FLUXNET (http://fluxnet.fluxdata.org/; Merbold et al., 2009), National Climatological Observatory of China Meteorological Administration (NCO-CMA), and the "Heihe Watershed Allied Telemetry Experimental Research (HiWATER)" (https://data.tpdc.ac.cn/zh-hans/special/heihe/; Liu et al., 2011; Li et al., 2013), respectively. The EC sites covered different ecosystem types, including forests (four sites), croplands (three sites), and grasslands (nine sites). The basic information about these EC sites can be found in Table S1. Due to the different durations of the EC sites, the time span of the EC-based ET observations ranged from 24 to 96 months (details in Fig. 1d). Based on standardized procedures (Vuichard and Papale, 2015) and the gap-filled method (Reichstein et al., 2005), quality control of the EC measurements was examined, and then we aggregated the EC-based half-hourly measurements to monthly values at each site for the BEPS ET validations on the monthly scale.

In addition, seven widely-used ET products (see Table 1 for details) were selected here to test the ability of BEPS to reproduce inter-annual fluctuations and trends in ET on national, first-level water resources region, and grid scales. Given the uncertainty of a single ET product, such evaluations were conducted based on the ensemble mean of these products (i.e., geometric mean). Furthermore, for matching temporal and spatial resolutions, all the ET products and the BEPS ET estimates were aggregated into the annual values and then were resampled to a spatial resolution of 0.25°. Finally, ET time series during 2001–2020 yearly were extracted for the whole vegetated Mainland China, each first-level water resources region, and each 0.25° grid, and the trends were estimated by the linear least square method.

In the present study, a relatively new, widely-used combined validation metric of the Kling–Gupta Efficiency (KGE; Gupta et al., 2012), which could measure overall performance, and meanwhile its three

Table 1
Overview of the selected seven widely-used ET products.

ET products	Spatio-temporal resolutions	Time span	Websites and references
Global Land Evaporation Amsterdam Model, Version 3.5a (GLEAM3.5a)	0.25° × 0.25°; daily	1980–2020	https://www.gleam.eu/; Miralles et al., (2011), Martens et al. (2017)
European Centre for Medium-Range Weather Forecasts Reanalysis-5 (ERA5)	0.25° × 0.25°; monthly	1979–present	https://cds.climate.copernicus.eu/cdsapp#!/dataset/reanalysis-era5-pressure-levels-monthly-means?tab=form; Hersbach et al. (2020)
ERA5-Land	~9 km × ~9 km; monthly	1950–present	https://cds.climate.copernicus.eu/cdsapp#!/dataset/reanalysis-era5-land?tab=form; Muñoz-Sabater (2019)
Modern Era Reanalysis for Research and Applications (MERRA), Version 2 (MERRA2)	2/3° × 1/2°; monthly	1980–present	https://disc.gsfc.nasa.gov/datasets?project=MERRA-2; Molod et al. (2015)
MERRA-Land	2/3° × 1/2°; monthly	1980–present	https://disc.sci.gsfc.nasa.gov/datasets?page=1&keywords=MERRA-land; Reichle et al. (2011)
Global Land Data Assimilation System Noah Land Surface Model L4, Version 2.1 (GLDAS_NOAH025_V2.1)	0.25° × 0.25°, monthly	2000–present	https://disc.gsfc.nasa.gov/datasets?keywords=GLDAS; Rodell et al. (2004)
Moderate-resolution Imaging Spectroradiometer global ET product, Version 6 (MOD16A2.006)	500 m × 500 m; 8-day	2001–present	https://e4ftl01.cr.usgs.gov/MOLT/; Running et al. (2017)

sub-components (i.e., R, β, and γ; details shown below) were also selected to evaluate the simulated ET by the BEPS model quantitatively. The formulas for KGE and the sub-components were written as,

$$
\begin{cases}
KGE = 1 - \sqrt{(R-1)^2 + (\beta-1)^2 + (\gamma-1)^2} & (1) \\[2mm]
R = \dfrac{\sum_{i=1}^{N}[(E_i - \mu_e)(O_i - \mu_o)]}{\sqrt{\sum_{i=1}^{N}(E_i - \mu_e)^2}\sqrt{\sum_{i=1}^{N}(O_i - \mu_o)^2}} & (2) \\[2mm]
\beta = \dfrac{\mu_e}{\mu_o} & (3) \\[2mm]
\gamma = \dfrac{\sigma_e/\mu_e}{\sigma_o/\mu_o} & (4)
\end{cases}
$$

where E_i is the simulated ET value from the BEPS of the ith data pair, while O_i is the reference ET value. μ_e and μ_o (σ_e and σ_o) represent means (standard deviations) of the BEPS and reference ET values, respectively. R is the correlation coefficient between the BEPS and reference ET. β is a metric to measure the average tendency of the BEPS ET larger (i.e., $\beta > 1$) or smaller than (i.e., $\beta < 1$) the reference, and the optimal value is 1. The sub-component of γ is used to examine the capacity of the BEPS ET

in reproducing variability of the reference data. The value of γ equal to 1 corresponds to the perfect performance, while values below (above) 1 represents the underestimated (overestimate) variability. The combined metric of *KGE* ranges from -∞ to 1, of which 1 suggests a perfect overall performance.

2.2.3. Identification of human-disturbed and natural vegetation

To in-depth understand vegetation changes and their impacts on ET and water yield, we considered whether human disturbances impact vegetation. According to Chen et al. (2019a) and Chen et al. (2021), we clustered vegetation types into two major groups, i.e., the human-disturbed (HD) vegetation, whose changes were mainly caused by anthropogenic disturbances, and the natural vegetation, whose changes were mainly driven by natural factors. Different from Chen et al. (2019a) and Chen et al. (2021), we also considered whether LC changed due to human activities during the study period. Here, LC changes (LCC) were defined as that at a given grid cell, the LC type in 2001 was replaced by others in any year of 2002–2020, i.e., LC type with at least one change during the study period. The regions with LCC across mainland China were extracted (Fig. S1). During 2001–2020, LCC happened over 18% of vegetated mainland China prominently clustered in southeastern mainland China, south-central Yellow River Basin (RB), northern Northwest RB, and western Songhuajiang RB. Area percentages with LCC varied among ten water resources regions, followed by larger ($> 17\%$) and smaller values ($< 16\%$) in southern and northern water resources regions, respectively. At last, we divided the vegetation types into three major groups: human-disturbed (HD)-LCC—HD vegetation with LCC, HD-Cropland—consistent cropland, and the natural vegetation—consistent non-agricultural LC during 2001–2020, despite some trees and grasses possibly planted for ecological restorations before 2001 (Chen et al. 2019a). Within the BEPS model, the characteristics of HD-Cropland and the natural vegetation were mainly reflected by LAI, while vegetation types and LAI were used to represent the characteristics of HD-LCC.

2.3. Temporal trends

The trends for climate variable, LAI, ET, and water yield were computed with the linear equation below:

$$v_i = at_i + b \tag{5}$$

where v_i and t_i (i=1,2,…,20) represent the target variable and the corresponding year, respectively; a is the temporal trend, but b is the intercept, and n is the sample size. Here, the least-squares method was employed to estimate the regression parameters (i.e., a and b). Throughout this study, the significance of the estimated trends was assessed using the Student's t-test with $p < 0.05$. Notably, for a given region (e.g., vegetated mainland China and each water resources region), the LAI, ET, and water yield trends of HD-LCC, HD-Cropland, and natural vegetation were the area-weighted values, i.e., the trends averaged over HD-LCC, HD-Cropland, and natural vegetation regions multiplied by the corresponding area percentage.

2.4. Attribution method and identification of dominant factors

The joint-solution method with multiple sensitivity numerical experiments developed by Sun et al. (2014, 2017, 2021) could successfully separate the respective impacts of each factor and was applied to attribute changes in hydrological variables and drought indices (i.e., linear trends and anomalies) on national and regional scales. Therefore, six numerical simulations were performed based on the concept and influential factors (i.e., precipitation, incoming solar radiation, temperature, relative humidity, and vegetation) of the BEPS ET (details in Table 2), including one control simulation and five experimental simulations. For the control simulation (EXP$_{CTL}$), the inputs were the original datasets (i.

Table 2
Details of the numerical experiments.

Experiments	Description
EXP$_{CTL}$	Daily climate variables, 8-day LAI, and annual LC maps during 2001–2020
EXP$_{PRE}$	All settings are the same as EXP$_{CTL}$, except that precipitation is fixed at the value of the year 2001. For example, the precipitation on June 1, 2001, is used for June 1 for every year from 2001 to 2020.
EXP$_{RAD}$	All settings are the same as EXP$_{CTL}$, except that incoming solar radiation is fixed at the value of the year 2001.
EXP$_{T}$	All settings are the same as EXP$_{CTL}$, except that temperature is fixed at the value of the year 2001.
EXP$_{RH}$	All settings are the same as EXP$_{CTL}$, except that relative humidity is fixed at the value of the year 2001.
EXP$_{VEG}$	All settings are the same as EXP$_{CTL}$, except that 8-day LAI and annual LC map are fixed at the value of the year 2001.

e., remaining their inter-annual changes) between 2001 and 2020. For each experimental simulation (EXP$_x$; x is for precipitation, incoming solar radiation, temperature, relative humidity, and vegetation), the x-factor from only 2001 (i.e., removing its inter-annual changes) and other factors from 2001 to 2020 were used. These five experimental simulations for precipitation, incoming solar radiation, temperature, relative humidity, and vegetation were referred to as EXP$_{PRE}$, EXP$_{RAD}$, EXP$_T$, EXP$_{RH}$, and EXP$_{VEG}$, respectively. Afterward, the contribution of each factor to the annual ET trends was estimated at each grid cell in the study area using the separation algorithm in *Appendix C*.

We re-evaluated this separation method on the grid cell scale before attributing ET and water yield trends and found that this method was effective across vegetated mainland China according to *R, β, γ*, and *KGE*. More details about the evaluation results can be found in Text S1 and Fig. S2. Based on the separated contributions of each factor and *Appendix C*, we can identify the dominant factors (including precipitation, incoming solar radiation, temperature, relative humidity, and HD-LCC, HD-Cropland, and natural vegetation) for the annual ET and water yield trends on grid cell, regional and national scales. It should be noted that the contributions of each factor to the annual water yield trends were estimated in terms of the water balance equation. In detail, the precipitation contributions to each grid cell's annual water yield trends were estimated by precipitation trend minus its contributions to the annual ET trend. In contrast, the contribution of the remaining factors was obtained by multiplying the factor's contribution to the annual ET trend by -1.00.

3. Results

3.1. Spatio-temporal trends in ET and water yield during 2001–2020

3.1.1. Evaluation of ET and water yield simulations with the BEPS model

The simulated ET and water yield by the BEPS model were evaluated against several independent datasets (Fig. 2). The monthly ET from the BEPS model agreed reasonably well with measurements from the flux sites (Fig. 2a), with $R = 0.89$ and $KGE = 0.72$, though the mean value and the temporal variability were slightly underestimated ($\beta = 0.91$) and overestimated ($\gamma = 1.24$), respectively. When we examined these metrics individually for each flux site (Fig. 2b), 12 out of the 16 EC sites showed β between 0.80 and 1.00, and γ between 1.10 and 1.40, while values of R and KGE were above 0.90 and 0.60, respectively.

The evaluation of ET and water yield over the selected 127 basins (Fig. 1d) was displayed in Fig. 2c and 2d, respectively. The BEPS model could reasonably capture the magnitudes and spatial patterns of the observed multi-year mean ET and water yield in these 127 basins with β, γ, and R all very close to 1.00. In addition, the BEPS model had a good overall performance based on the integrative validation metric of KGE above 0.85.

The BEPS ET was also evaluated against the ensemble mean of seven widely-used ET products from the perspectives of inter-annual
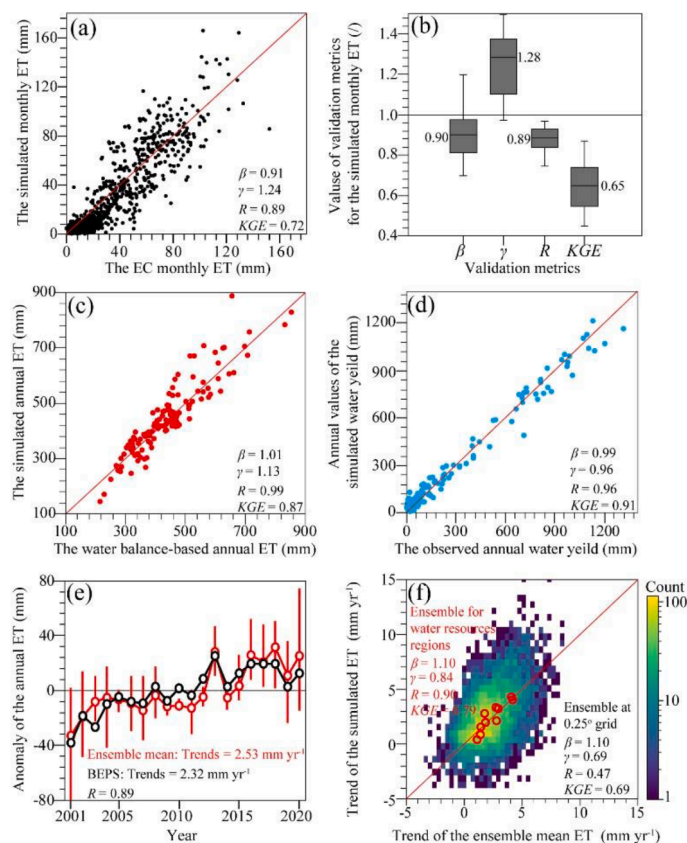
Fig. 2. Evaluation of simulated ET and water yield by the BEPS model. (a) Scatterplots of simulated monthly ET against monthly ET derived from 16 EC flux sites. (b) Boxplots for the model performance metrics of monthly ET simulations at 16 EC flux sites. In this panel, the whiskers represent the minimum and maximum values of the model performance metrics. The outer edges of the boxes and the horizontal lines within the boxes indicate the 25th, 75th, and 50th percentiles (also shown with numbers) of the model performance metrics. (c) Scatterplots of the simulated versus the water balance-based multi-year (2001–2010) mean annual ET on 127 validation basins. (d) Scatterplots of the simulated versus the water balance-based multi-year (2001–2010) mean annual water yield on 127 validation basins. (e) Comparison of the inter-annual fluctuations of the BEPS model and the ensemble mean annual ET in vegetated mainland China during 2001–2020. The red vertical lines suggest the range of the selected seven ET products. (f) Scatterplots of the BEPS versus the ensemble mean annual ET trends over ten water resources regions and at all the 0.25° grids.

fluctuations and long-term trends (Fig. 2e, and 2f). The inter-annual fluctuation of the simulated ET over vegetated mainland China closely agreed with the ensemble mean ($R = 0.89$). The long-term trends in ET derived from the BEPS model and ensemble mean also agreed very well, i.e., 2.32 mm y^{-1} from the BEPS versus 2.53 mm y^{-1} from the ensemble mean. When it came down to the water resources regions (0.25° grid), the magnitudes and spatial variabilities of the ET trends were overestimated and underestimated by the BEPS model, respectively, with β of 1.10 (1.10) and γ of 0.69 (0.84). The R and KGE values greater than 0.40 suggested that the model could capture the ET trends on regional and 0.25° grid scales (Fig. 2f). Overall, the above evaluation indicated that the performance of the BEPS model was reasonably well in simulating ET and water yield, which gave us confidence in the following sensitivity experiments.

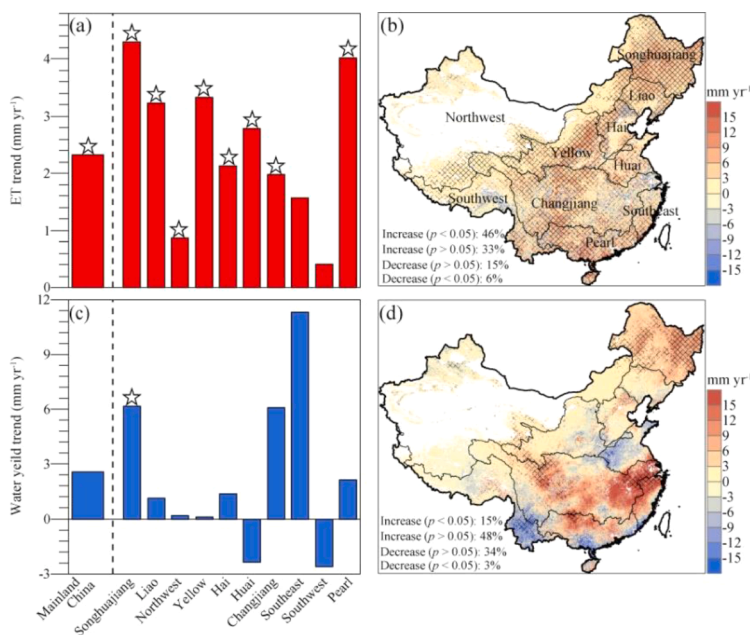*3.1.2. Trends in ET and water yield*

As seen from Fig. 3a (Fig. 3c), the vegetated mainland China annual ET (water yield) values averaged from 2001 to 2020 were 409.05 mm (301.74 mm), and showed clear regional differences, ranging from 205.98 mm for Northwest RB to 635.91 mm for Southeast RB (from 50.97 mm for Songhuajiang RB to 920.77 mm for Southeast RB). Spatially, the multi-year mean annual ET and water yield were mainly characterized a decreasing tendency from southeast to northwest China, with a range from more than 1000 mm to lower than 100 mm for ET, and from more than 1000 mm to lower than 5 mm for water yield (Fig. 3b, and 3d).

The trends of ET and water yield over different water resources regions during 2001 and 2020, as well as their spatial distributions across vegetated mainland China, are depicted in Fig. 4. On average, a significant ($p < 0.05$) increasing ET trend (2.32 mm y^{-1}) was detected over vegetated mainland China (Fig. 4a). Spatially, 46% of the study area experienced significant ($p < 0.05$) upward trends of ET, with the highest values (> 6.00 mm y^{-1}) mainly observed in central, northeast, and southeast China (Fig. 4b). Significant ($p < 0.05$) decreasing trends in ET were observed over 6% of vegetated mainland China, primarily in southern China. When it came to the region-averaged trend in ET (Fig. 4a), eight out of ten water resources regions experienced significant ($p < 0.05$) increases in ET, with the strongest increase (> 4.00 mm y^{-1}) found in Songhuajiang RB located in the most northeastern China.

The annual water yield averaged over vegetated mainland China increased by 2.56 mm y^{-1} ($p > 0.05$) during 2001–2020 (Fig. 4c). Although the trends in water yield seemed stronger than those in ET (Fig. 4b and 4d), the trends in water yield were insignificant ($p > 0.05$) over 80% of vegetated mainland China (Fig. 4b). Significant ($p < 0.05$) trends in water yield were detected over only 18% areas (15% for an increase and 3% for a decrease). When it involved the regionally averaged trend in water yield (Fig. 4c), only Songhuajiang RB from most of northeastern China experienced a significant ($p < 0.05$) increase trend in water yield ($\sim$6 mm y^{-1}).
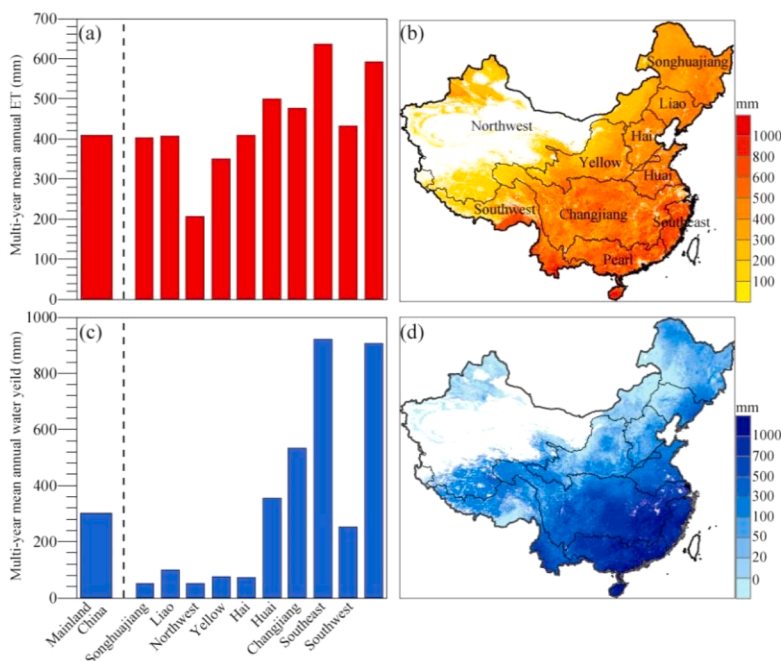
Fig. 3. Multi-year mean annual ET and water yield during 2001–2020. (a) Multi-year mean annual ET averaged over vegetated mainland China and the ten water resources regions. (b) Spatial pattern of multi-year mean ET across vegetated mainland China. (c) Multi-year mean annual water yield averaged over vegetated mainland China and the ten water resources regions. (d) Spatial patterns of multi-year mean water yield across vegetated mainland China.

Fig. 4. Trends for annual ET and water yield during 2001–2020. (a) Trends for annual ET averaged over vegetated mainland China and each water resource region. (b) Spatial pattern of annual ET trends across vegetated mainland China. (c) Trends for annual water yield averaged over vegetated mainland China and each water resource region. (d) Spatial pattern of annual water yield trends across vegetated mainland China. In (a) and (c), the star represents significant ($p < 0.05$) trends. In (b) and (d), the dashed area indicates significant ($p < 0.05$) trends, and the area percentage with downward and upward trends of ET and water yield is shown in the bottom left corner.

## 3.2. Spatio-temporal trends in climate variables and vegetation during 2001–2020

3.2.1. Trends in climate variables

The trends of four climate variables (i.e., precipitation, radiation, temperature, and relative humidity) over each water resources region during 2001 and 2020, as well as their spatial distributions are shown in Fig. 5. The annual precipitation averaged over vegetated mainland China showed a significant ($p < 0.05$) increase trend of 5.05 mm y^{-1} during 2001–2020 (Fig. 5a). Spatially, precipitation increased over 79% of vegetated mainland China, and 25% areas corresponded to significant ($p < 0.05$) increases, mainly in northeast and central-west China

(Fig. 5b). The strongest increases in precipitation were detected in northeast and southeast China, while the decreases were mainly observed in the southwesternmost part of China. Regionally, precipitation increased over nine out of ten water resources regions (except Southwest RB) with significant trends over Liao, Yellow, and Changjiang RB (Fig. 5a).

The annual incoming solar radiation over vegetated mainland China experienced a decreasing trend (8.56 MJ m^{-2} y^{-1}, $p < 0.05$) during 2001–2020 (Fig. 5c). Spatially, 36% of vegetated mainland China witnessed increasing incoming solar radiation, and only a small portion showed significant ($p < 0.05$) increases (Fig. 5d). On the other hand, nearly two-thirds (64%) of vegetated mainland China experienced
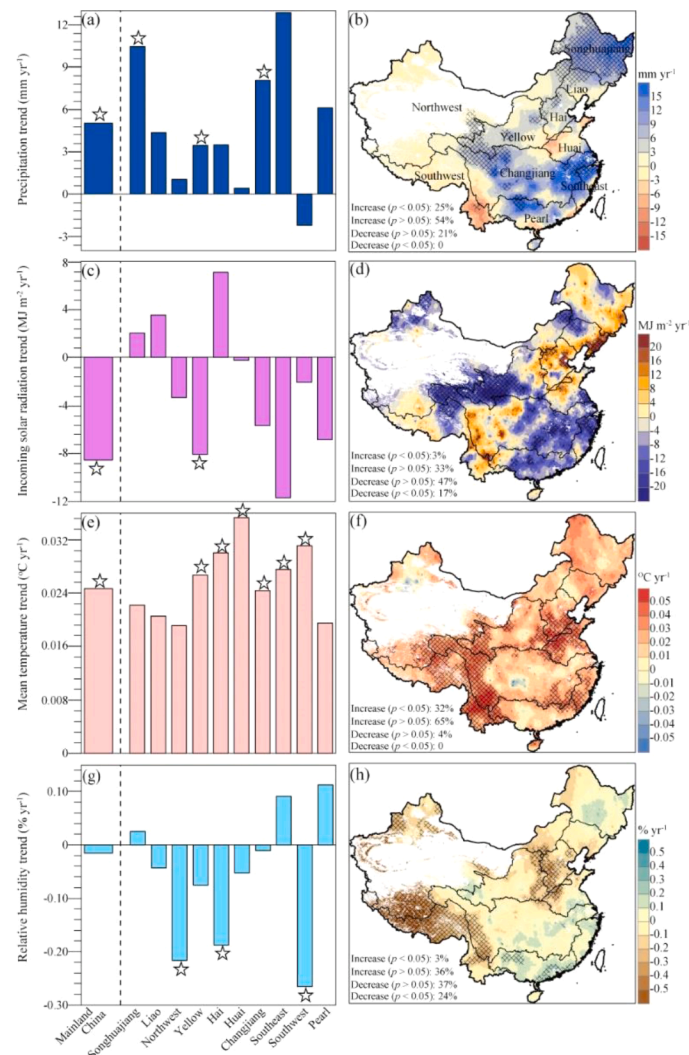
Fig. 5. Annual trends in the major climate variables during 2001–2020. The left column is for trends of the annual region-averaged (a) precipitation, (c) incoming solar radiation, (e) mean temperature, and (g) relative humidity. The stars represent significant ($p < 0.05$) trends. The right column shows the spatial patterns of trends in annual average (b) precipitation, (d) incoming solar radiation, (f) mean temperature, and (h) relative humidity across vegetated mainland China. The dashed area represents significant ($p < 0.05$) trends. The area percentage with downward and upward trends of these climate variables is also presented in each panel.

reductions in incoming solar radiation, with significant ($p < 0.05$) decreases over 17% of the study area. These significant ($p < 0.05$) decreases were mainly found in Yellow RB, which is located in central-west China (Fig. 5d). However, the incoming solar radiation decreased over six out of ten water resources regions. The significant ($p < 0.05$) decreasing trend was only found over Yellow RB (Fig. 5c).

The mean temperature for vegetated mainland China had a significant ($p < 0.05$) warming trend of 0.025 °C y^{-1} (Fig. 5e). Spatially, 97% of vegetated mainland China witnessed increasing trends in temperature during 2001–2020, and 32% of the study area experienced significant ($p < 0.05$) increases, primarily located in the southwest, north and southeast China (Fig. 5f). In addition, six out of ten water resources regions experienced significant ($p < 0.05$) increasing trends in temperature (Fig. 5e).

The annual nation-averaged relative humidity trend during 2001–2020 was close to zero (Fig. 5g), although there were strong spatial variations in the trends in relative humidity (Fig. 5h). Nearly three-quarters of the country had insignificant trends in relative humidity (Fig. 5h). On the other hand, one-quarter of the country witnessed significant ($p < 0.05$) decreases in relative humidity, mainly over southwest and north China, i.e., Southwest RB, Northwest RB and Hai

RB (Fig. 5g).

3.2.2. Trends in LAI

The trends in LAI over different water resources regions during 2001 and 2020, as well as their spatial distributions, are illustrated in Fig. 6. The annual nation-averaged LAI experienced a significant ($p < 0.05$) greening trend of 0.015 m^2 m^{-2} y^{-1} during the past two decades (Fig. 6a). The widespread greening trends were observed over ~80% of vegetated mainland China, with more than half of the study area showing significant ($p < 0.05$) greening trends (Fig. 6b). Conversely, only 7% of vegetated mainland China experienced significant ($p < 0.05$) browning trends (i.e., decreases in LAI), which were mainly found in southern parts of China.

All ten water resources regions experienced significant ($p < 0.05$) greening trends with the minimum increase in Northwest RB and maximum increase in Pearl RB (Fig. 6a). To further examine what (e.g., human activities and natural factors) caused the greening trends at the regional averaged scale, we broke vegetation down into human-disturbed vegetation (HD-LCC and HD-Cropland) and natural vegetation and then calculated their corresponding LAI trends (Fig. 6a). The nation-averaged HD-LCC, HD-Cropland and natural vegetation LAI
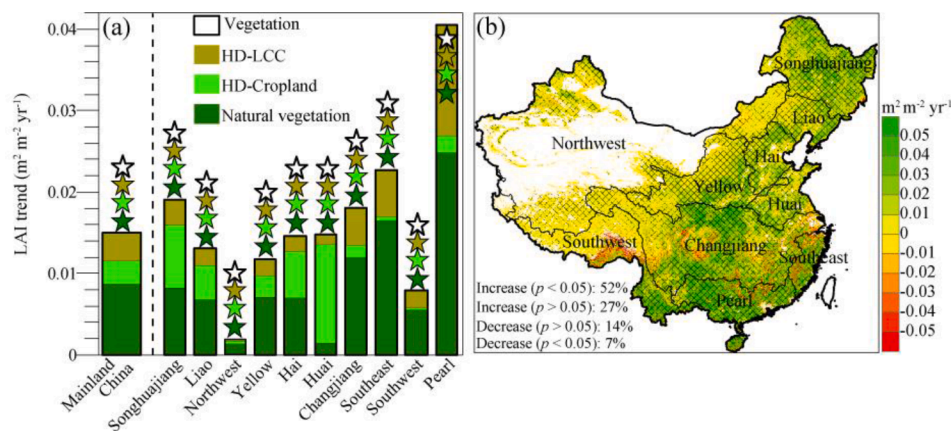
Fig. 6. (a) Vegetation LAI trends for vegetated mainland China and each water resources region, accompanied by HD-LCC, HD-Cropland, and natural vegetation LAI trends. The star represents significant ($p < 0.05$) trends. (b) Spatial distribution of LAI trends across vegetated mainland China. The area percentage for downward and upward trends of LAI is shown in the bottom left corner.

significantly ($p < 0.05$) increased by 0.0035, 0.0029, and 0.0089 $\mathrm{m^2\,m^{-2}}$ $\mathrm{y^{-1}}$, respectively. This indicated that the natural vegetation played a decisive role in the significant ($p < 0.05$) greening trends over mainland China (Fig. 6a). One exception was Huai RB where the trend in HD-Cropland dominated its regional LAI increase (Fig. 6a), suggesting that the significant ($p < 0.05$) greening in this region was closely associated with intensive agriculture management practices.

3.3. Attributions for the trends in ET and water yield

3.3.1. Attributions for the trends in ET
When considering vegetated mainland China as a whole (Fig. 7a, 7c, 7e, 7g, and 7i), precipitation and vegetation contributed similarly to the ET trends (1.20 mm $\mathrm{y^{-1}}$ for precipitation versus 1.29 mm $\mathrm{y^{-1}}$ for vegetation). Among three types of vegetation, i.e., HD-LCC, HD-Cropland, and natural vegetation, the natural vegetation made the largest contribution (0.56 mm $\mathrm{y^{-1}}$). However, the contributions of incoming solar radiation (-0.20 mm $\mathrm{y^{-1}}$), temperature (0.33 mm $\mathrm{y^{-1}}$), and relative humidity (-0.33 mm $\mathrm{y^{-1}}$) were much lower than precipitation and vegetation.

Regarding the level of water resources regions, the contributions of precipitation were positive for nine out of ten water resources regions, with a decreasing tendency from northeast to southwest China (Fig. 7a and 7b). The Southwest RB was the only water resources region where the contribution of precipitation to ET trends was negative (-0.63 mm $\mathrm{y^{-1}}$). Incoming solar radiation made negative contributions over ~70% of vegetated mainland China and over nine of ten water resources regions (except Huai RB) (Fig. 7c and 7d). The temperature positively contributed to ET trends during 2001–2020 for all ten water resources regions, and the most substantial contributions are observed over the southwest part of China (Fig. 7e and 7f). The contributions of relative humidity were dominantly negative with strong spatial variations (Fig. 7g and 7h). The strongest negative contributions (~-1.00 mm $\mathrm{y^{-1}}$) were observed in northeastern and southeastern China. As for the influences of vegetation dynamics on ET trends, their contributions were dominantly positive over all water resources regions, as well as over 70% of vegetated mainland China (Fig. 7i and 7j). The highest contribution was observed in Pearl RB located in southeastern China (> 3.50 mm $\mathrm{y^{-1}}$), while the lowest contribution was observed in western China (< 0.50 mm $\mathrm{y^{-1}}$). Over other water resources regions, the contributions of vegetation dynamics were generally between 0.50 mm $\mathrm{y^{-1}}$ and 2.00 mm $\mathrm{y^{-1}}$. Among three vegetation types (Fig. 7i), the HD-LCC and the HD-Cropland played a major role over Southwest and Pearl RB, and Liao, Hai, and Huai RB, respectively, whereas the natural vegetation was more important over other water resources regions.

The spatial distribution of the dominant factor for ET trends over each grid cell is shown in Fig. 8. Regionally, precipitation and vegetation (including HD-LCC, HD-Cropland, and natural vegetation) together dominate nine out of ten water resources regions, and the temperature was the driver for ET trends in Southwest RB. In terms of area coverage, precipitation and vegetation were the dominant factors over 32% and 55% (16% for HD-LCC, 9% for HD-Cropland, and 30% for natural vegetation) of vegetated mainland China. Precipitation mainly dominated the ET trends in northern China, whereas vegetation played a more important role in the south. In addition, the region dominated by temperature was about 8%, primarily in southwestern China.

3.3.2. Attributions for the trends in water yield
Fig. 9 shows the contribution of precipitation to water yield trends over vegetated mainland China during 2001 and 2020, as well as their average contributions for different water resources regions. When considering vegetated mainland China as a whole, the contribution of precipitation to water yield trends during 2001–2020 was 3.85 mm $\mathrm{y^{-1}}$. In addition, the contribution of precipitation was positive for eight out of the ten water resources regions, ranging from 0.4 mm $\mathrm{y^{-1}}$ in Northwest RB to 11.45 mm $\mathrm{y^{-1}}$ in Southeast RB (Fig. 9a). The Huai RB and Southwest RB were the only exception with negative contributions, which might be associated with more precipitation being allocated to ET (Fig. 8a). In terms of percentage of areas, positive precipitation contributions were found over three quarters (76%) while negative contributions covered 24% areas, mainly in southwestern and central-east China (Fig. 9b).

The dominant factor driving annual water yield trends over each water resource region, as well as spatial distribution of the dominant factor, is illustrated in Fig. 10. Precipitation was the driver for water yield trends for nine out of ten water resources regions, while HD-LCC was the dominant factor for Huai RB. Spatially, precipitation dominated 64% of vegetated mainland China, while vegetation dominated 30%, mainly located in northern China. Incoming solar radiation, temperature, and relative humidity combined accounted for 6%, primarily over southwestern China.

4. Discussion

4.1. Result comparison and possible explanations for spatial differences in the dominant factors controlling trends in ET and water yield

Our study found the effects of increased (decreased) ET but decreased (increased) water yield due to vegetation greening (browning) across vegetated mainland China, which is consistent with results
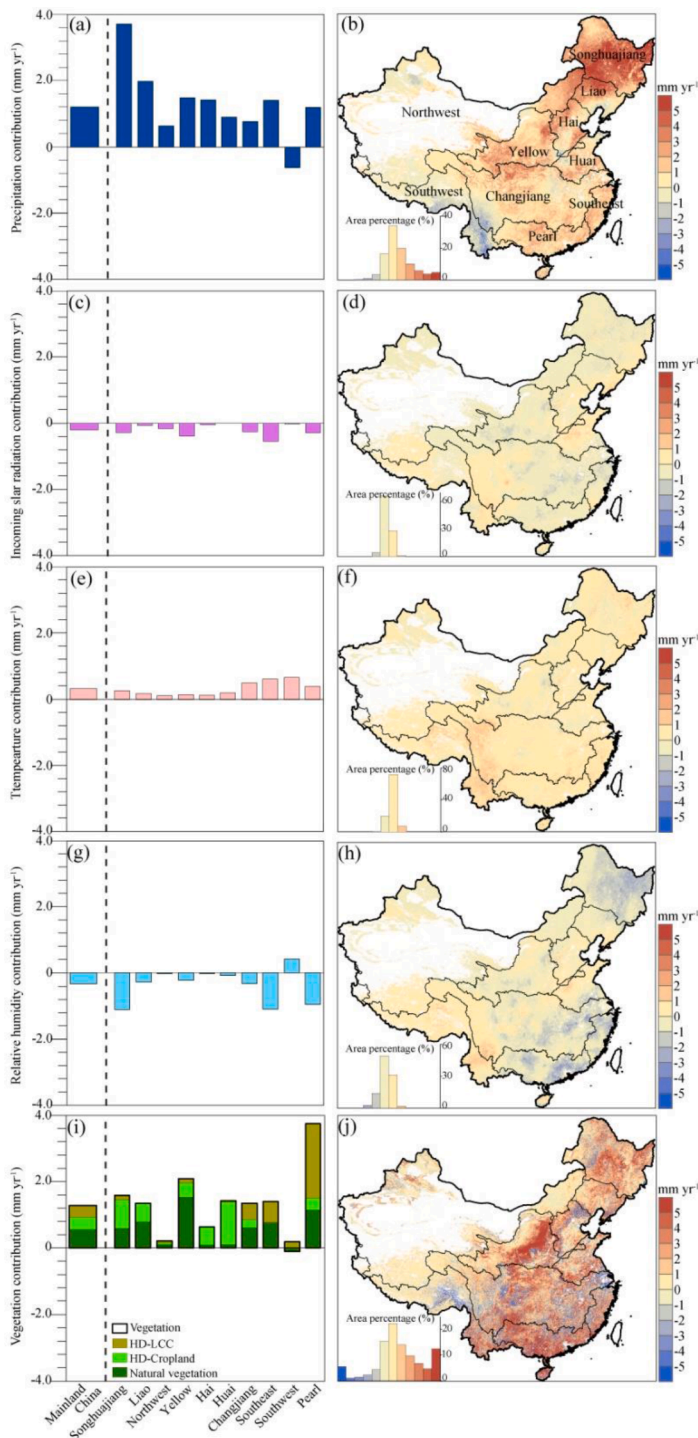
Fig. 7. Contributions of each driving factor to the annual ET trends during 2001–2020. The left panel is for contributions of precipitation (a), incoming solar radiation (c), mean temperature (e), relative humidity (g), and vegetation (i) for vegetated mainland China and ten water resources regions. The right panel is spatial patterns for contributions of precipitation (b), incoming solar radiation (d), mean temperature (f), relative humidity (h), and vegetation (j) across vegetated mainland China. In the right panel, the inset histogram shows the area percentages stratified by the contributions.

based on paired-catchment experiments (Brown et al., 2005; Yurtseven et al., 2017) and numerical simulations (Liu et al., 2016b; Bai et al., 2020; Xie et al., 2020; Zhang et al., 2020) in other regions. Notably, the vegetation greening effects on ET and water yield varied in space. Taking central-east Yellow and central-south Pearl RB as an example, the vegetation greening-induced increases (decreases) in ET (water yield) were larger than 5.00 mm y^{-1} (smaller than -5.00 mm y^{-1}), despite apparent differences in the LAI increases between the two sub-regions (i.e., generally < 0.03 y^{-1} for the former versus > 0.03 y^{-1} for the latter). The evident spatial variations of vegetation greening effects may be explained by the product of the ET or water yield sensitivity (generally referred to as the change in the dependent variable per unit change in a specific independent variable) to annual LAI and the trends in annual LAI. Some researchers have argued that the sensitivity of ET and water yield to vegetation greening depends largely on the climatic background (Sun et al., 2014; Feng et al., 2016; Bai et al., 2020; Zhang et al., 2020, 2021b), i.e., more sensitive in water-limited areas (e.g., central-east Yellow RB) than in energy-limited areas (e.g., central-south Pearl RB) (Feng et al., 2016; Bai et al., 2020). Therefore, the greater contributions of vegetation greening over the central-east Yellow RB might be due to the greater sensitivity of ET (water yield) to annual LAI. In addition, the contribution of natural vegetation averaged over Southwest RB was negative but small, despite its corresponding increases in LAI. This also could be attributed to the larger negative
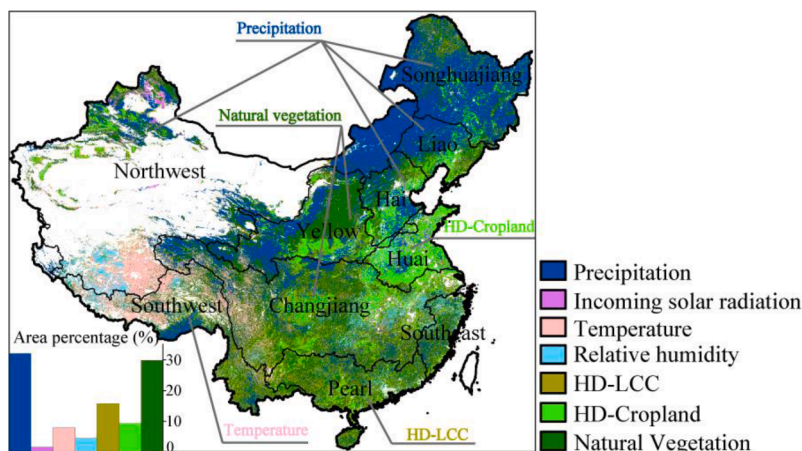
Fig. 8. Spatial distributions of dominant factors of the annual ET trends across vegetated mainland China. The inset histogram shows the area percentages stratified by the dominants.
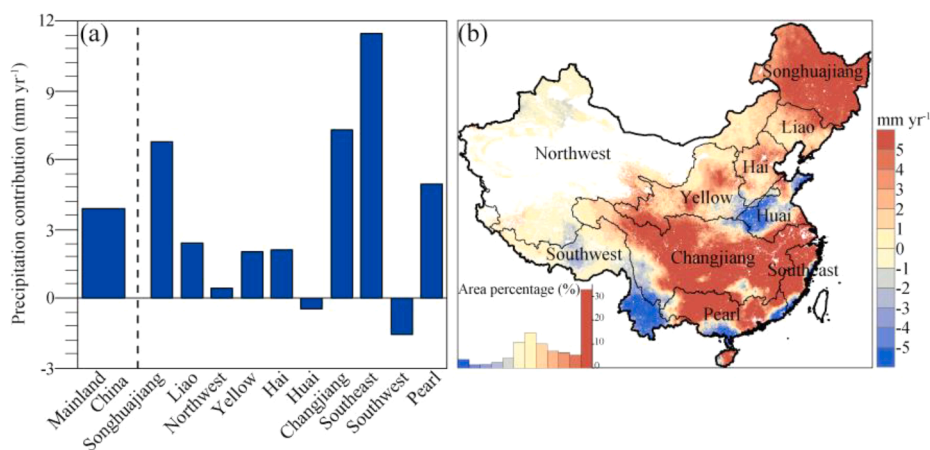

Fig. 9. Contributions of precipitation to the annual water yield trends from 2001 to 2020. (a) Contributions of precipitation for vegetated mainland China and ten water resources regions. (b) Spatial patterns for contributions of precipitation across vegetated mainland China. In (b), the inset histogram shows the area percentages stratified by the contributions.
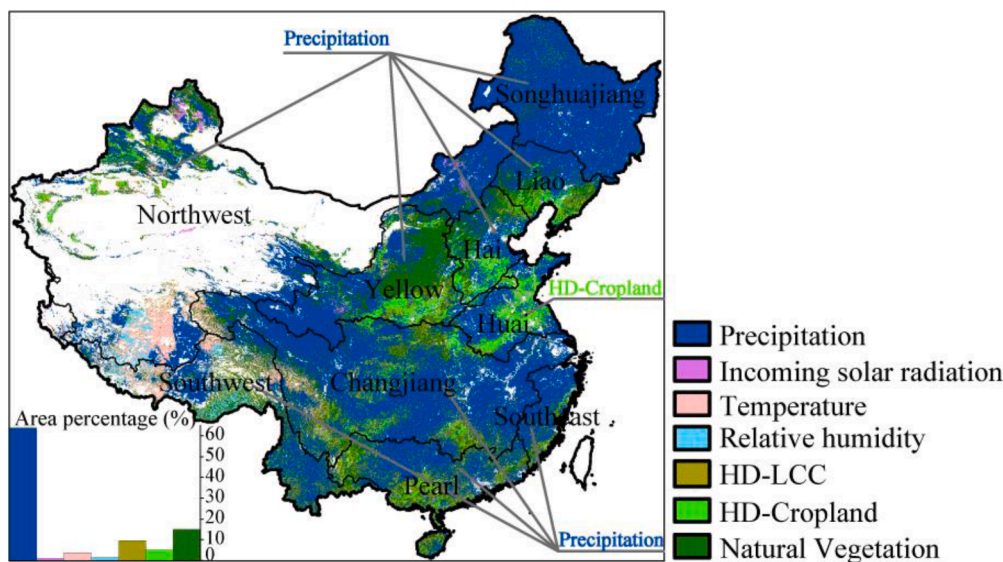

Fig. 10. Spatial distributions of dominant factors of the annual water yield trends across vegetated mainland China. The inset histogram shows the area percentages stratified by the dominants.

contributions over central-south Southwest RB (compared to the remaining regions), where ET was more sensitive to vegetation greening due to the higher aridity and the larger decreases in LAI ($< -0.04 y^{-1}$) existed.

In this study, we identified that precipitation was the primary factor for the ET trends in northern China, while temperature/relative humidity was clustered in southwestern Northwest RB. Furthermore, the dominant factor regulating the water yield trends was precipitation in most of vegetated mainland China but vegetation in central and eastern China. Overall, the findings were similar to several case studies (e.g., Meng et al. 2020, Lin et al. 2021, Wang et al. 2021, Ma and Zhang 2022). For instance, the ET trends were controlled mainly by precipitation in the Three-North region of China (Meng et al., 2020) and most of the Tibetan Plateau (Ma and Zhang, 2022), and temperature/vapor pressure deficit in the western Tibetan Plateau (Lin et al., 2021), while the vegetation change played a dominant role in reducing runoff in most of Yellow RB (Wang et al., 2021).

4.2. Implications for water management and ecological restoration engineering

In this study, we found that precipitation changes were beneficial to the increase in potential water resources (i.e., increased water yield) over 76% of vegetated mainland, where precipitation generally played a dominant role. Therefore, we should note that the increased precipitation potentially increased the risk of water redundancy-related disasters (e.g., floods) in some regions, i.e., eastern parts of southern water resources regions with the larger contributions (> 5.00 mm y^{-1}) of precipitation. Additionally, 24% of vegetated mainland China had negative contributions to precipitation. This suggested that the decrease in precipitation would like to increase the risk of water shortage in these regions, especially in the northwest of the Northwest RB (a typical arid area) and in most of the Huai RB (one of the major agricultural production bases). All in all, our quantitative analyses of the impacts of precipitation on water yield trends in space provided an important reference for mitigating the risk of water redundancy-related disasters and water shortage in some regions, e.g., by implementing water division projects via transferring water from regions with redundant to water-scarce regions.

Our analyses and previous findings (e.g., Teuling et al. 2013, Tian et al. 2017, Bai et al. 2020, Zhang et al. 2021a, 2021b) showed that vegetation greening caused more water consumption (i.e., increased ET and decreased water yield) and might increase the risk of water scarcity in most of northern China. Nevertheless, different regions showed different water yield responses to vegetation changes. Such quantitative analysis results were relevant to reduce the risk of water shortages. Our analyses suggested that vegetation greening played a key role in regulating changes in ET over most of vegetated mainland China and might increase water consumption in cultivated regions (e.g., eastern Hai RB, south-central Yellow RB, and most of Huai RB). Moreover, the major contributor to the decrease in water yield was vegetation over 30% of vegetated mainland China. This implied that the vegetation greening had increased stress on the water supply over these regions despite increased precipitation. As a result, it was urgent for these regions to reasonably allocate the limited water resources and implement water-saving measures for alleviating the regional water resource utilization issues. Vegetation greening could also negatively impact the downstream water supply via runoff generation and flow concentration processes (Tian et al., 2017). For example, the vegetation greening in the upper Han River basin (a basin in northern-central Changjiang RB) introduced an average decrease of 77% of the intended annual water diversion volume of the South-to-North Water Diversion Project (Zhang et al., 2021b).

Although the vegetation greening has brought about positive ecosystem goods and services, in some regions, it could result in negative impacts on water resources, mainly for arid and semi-arid regions (Yu et al., 2010). Our results confirmed such negative impacts, i.e., a decrease in water yield in 30% of vegetated mainland China dominated by vegetation greening, and further implied that ecological restoration engineering should consider the negative impacts of vegetation greening on water resources. We can use several management measures to balance ecological and hydrological benefit tradeoffs to cope with this issue. For example, thinning and understory control can produce more water from the soil for groundwater recharge and downstream users and increase the amount of available water to the remaining vegetation (Sun et al., 2015; Caldwell et al., 2015). Besides, with a thorough consideration of local environmental conditions, managers can select the appropriate vegetation species (i.e., less water need and higher ecosystem benefits) to modify the existing vegetation structure and composition, optimizing the tradeoffs between ecological and hydrological benefits (Cao et al., 2011; Tian et al., 2017; Bai et al., 2020; Xie et al., 2020).

4.3. Uncertainties

The results may involve uncertainties from various sources, such as the structures, parameterizations, and inputs of the BEPS model and attribution methods. Therefore, these uncertainties are discussed in the following sections.

4.3.1. Uncertainties in model structures and parameterizations of the BEPS model

A Jarvis-type stomatal conductance module was used within the BEPS model (Chen et al., 1999) to describe the impacts of environmental conditions (i.e., temperature, vapor pressure deficit, solar radiation, and soil moisture content) on plant physiological characteristics (i.e., stomatal conductance). Despite the better performance of the Jarvis-type modules in simulating the impacts of environmental conditions on water and carbon fluxes (Jarvis, 1976; Lhomme, 2001; Wang et al., 2020), the interactive effects between environmental factors on stomatal conductance are not taken into account. If each environmental factor is not independent, it potentially biases the estimated stomatal conductance (Damour et al., 2010). Moreover, the Jarvis-type stomatal conductance module within the BEPS model does not involve elevated CO_2-induced stomatal conductance changes. Generally, there is a common view that in response to the elevated CO_2, the stomatal conductance is likely to decline but with different rates among plant types (Norby et al., 2005; Gray and Brady, 2016; Hiyama et al., 2017). Correspondingly, plant transpiration and even ecosystem ET decrease, and at last, the water cycle on both regional and global scales changed (Gedney et al., 2006; Sun et al., 2014; Yang et al., 2019). The accuracy of our results based on the BEPS model may be impacted by the unidirectional coupling between vegetation and water and carbon fluxes, and the lack of high CO_2-induced stomatal resistance decreases.

The BEPS model does not account for lateral movement of soil water, cryospheric hydrological processes, lakes, and reservoirs, and anthropogenic water use interventions (e.g., farmland irrigation, groundwater withdrawal, and the inter-basin water transfer projects), although they are pivotal to accurately conduct eco-hydrological simulations (Jansson et al., 2003; Ju et al., 2010a, 2010b; Galleguillos et al., 2011; Li et al., 2018; Gao et al., 2019; Zhai and Tao, 2021). Lateral movement of soil water can redistribute soil water content according to topographical characteristics and soil water gradients (Gao et al., 2003; Senatore et al., 2015). In general, water lateral movement increases ET but decreases runoff, and these effects are evident, especially under unsaturated soil and steep morphology conditions (Senatore et al., 2015; Rummler et al., 2019). As a result, neglecting this process leads to underestimations (overestimations) of the simulated ET (water yield). As an important component of surface water resources, glacier meltwater positively contributes to runoff from glaciated regions. Such a positive contribution increases with intensified global warming-induced glacier shrinkage (Jansson et al., 2003; Xu et al., 2015; Li et al., 2018),

suggesting that the lack of cryospheric hydrological processes is likely to underestimate water yield as well as its increases. Besides, biases of the hydrological variables simulated by the BEPS model can be caused by no incorporation of lakes and reservoirs because they can regulate water storage to change the magnitude and timing of runoff (Mao et al., 2016; Zajac et al., 2017). For instance, lakes with dramatic changes in China (especially in the northern provinces) have led to significant changes in the regional water budget, including ET and runoff (Zhou et al., 2015; Tao et al., 2020).

Irrigation is an important land management approach to modify energy allocation and change the surface water balance through supplementing soil moisture, especially in water-limited regions (e.g., West and North China; Han et al., 2011; Lei et al., 2014; Chen and Dirmeyer, 2018; Li et al., 2016, 2017, 2018; Wang et al., 2021; Zhang et al., 2021c). Both observations and numerical simulations confirm such impacts as increased ET amount, altered ET trends, reduced runoff, and intensified local water cycles (Li et al., 2007; Lei et al., 2014; Chen and Dirmeyer, 2018; Zhang et al., 2021c). Therefore, ignoring irrigation may lead to underestimations of ET and water yield and biased trends over irrigated regions. Similarly, groundwater withdrawals and inter-basin water transfer projects can also change the surface water balance by regulating soil moisture (Vörösmarty and Sahagian, 2000; Govind et al., 2011; Li et al., 2018; Zhang et al., 2019). For example, the South-to-North Water Transfer Project in China can increase top-layer soil moisture, ET, and runoff in the water intake areas due to the impact of injecting water (Chen and Xie, 2010; Zou et al., 2016) but may exert the opposite impacts in the water delivery areas. The excessive groundwater extraction on the North China Plain has lowered groundwater tables, reduced soil water content, and affected vegetation roots' absorption (Wang et al., 2022).

The lateral movement of soil water, hydrological processes in the cryosphere, lakes and reservoirs, and anthropogenic water use interventions are closely associated with the spatio-temporal dynamics of soil moisture, which determine ET processes and water balance. Some studies have pointed out that vegetation indices (e.g., LAI) can be used to represent soil moisture stress on ET processes and even, to some extent, water balance (Droogers et al., 2010; Shen et al., 2013; Lei et al., 2014; Mu et al., 2007). Therefore, using LAI data in the BEPS model can partly reflect the impacts of soil moisture on ET and water yield and potentially reduce simulation uncertainties. However, it should be noted that vegetation indices may not fully reflect the stress of soil moisture. For example, temporal variations in soil moisture have a lagged effect on the dynamics of LAI, suggesting that although soil moisture and ET change rapidly, the LAI will remain stable for a short duration. As a result, using only the LAI as an alternative to represent the stress of soil moisture, the ET and water yield estimates are likely to introduce more or less uncertainties in our study. Moreover, our findings differ from previous studies (e.g., Zhang et al. 2018, 2020), e.g., the factors contributing to the ET trends in the eastern part of southern water resources regions. This study attributed to vegetation, while Zhang et al. (2020) attributed to climatic factors, which may be due to differences and uncertainties in structures, parameterizations, and simplifications of the models.

4.3.2. Other uncertainties

The uncertainties in the input datasets (i.e., meteorological, LAI, and LC datasets) can be propagated to the simulation results. Uncertainties in the gridded meteorological fields (Ju et al., 2010a, 2010b; Sun et al., 2021) affect the accuracy of the simulations due to the uneven spatial distribution of weather sites and the spatial variability of the interpolated climate variables themselves (e.g., precipitation tends to have significant spatial variability, especially near complex terrains; Sun et al., 2020). Previous studies argued that different LAI products had different magnitudes of dynamics, including MODIS, GLASS, GLOBMAP, and GIMMS (Jiang et al., 2017; Liu et al., 2018; Fang et al., 2019; Chen et al., 2021), but they all showed an increase in LAI after the year 2000

(Chen et al., 2019b, 2021). The impacts of the GLOBMAP uncertainties on our conclusions might be limited, mainly because the focus of this study was on ET and water yield trends, and the GLOBMAP and GIMMS datasets (currently updated to 2015 at present) have been noted to be more suitable for long-term ET simulations (Chen et al., 2019b). Although the accuracy of MCD12Q1 V006 has improved relative to the previous version V005 (Sulla-Menashe et al., 2019), 1.6% of the global land still has fake land cover changes. Thus, examining vegetation type changes based on the MCD12Q1 V006 LC might increase the uncertainty of our findings. Moreover, using the 2019 LC as an alternative to the 2020 LC can lead to uncertainties.

The combination of multiple interacting biogeochemical drivers and land-use effects has resulted in significant changes in vegetation structure and function worldwide (Zhu et al., 2016). Among these drivers, climate change, such as anthropogenic warming and regional trends in precipitation, is believed to be a non-ignorable driver of the global greenness changes and dominates such changes over 28% of the global vegetated area (Zhu et al., 2016). In turn, vegetation changes can feed back to the climate through biogeochemical and biogeophysical processes (Piao et al., 2020). Studies have suggested that vegetation greening can alter the water and energy exchanges between the land and the atmosphere, affecting the atmospheric circulation patterns and finally changing various meteorological variables (e.g., temperature and precipitation) on local and regional scales (Pielke, 2005; Sheil and Murdiyarso, 2009; Zeng et al., 2017; Yosef et al., 2018; Yu et al., 2021). All in all, there existed two-way interactions between vegetation and the atmosphere. This implies that the contributions of vegetation (climate change) to the ET and water yield trends in this study partially involves the effects of climate change (vegetation), leading to uncertainties in our results. Another limitation comes from the separation method utilized in this study. The relationships between the water cycle, climate variables, and vegetation dynamics are complex. In this study, linearly adding their contributions may introduce some uncertainties to our results. Notwithstanding such shortcomings, this new separation method is generally prior to traditional separation methods [e.g., the sensitivity method in Zhang et al. (2020) and the differential equation approach in Zhang et al. (2018)]. Therefore, the choice of the attribution method is another possible reason for the different factors contributing to the ET trends in the eastern part of southern water resources regions between our findings (i.e., vegetation) and previous studies (e.g., climatic factors; Zhang et al., 2020).

5. Conclusions

In this study, we decomposed how climate variables and vegetation (both human-disturbed and natural vegetation) impacted the annual ET and water yield trends across vegetated mainland China during 2001–2020, based on a series of sensitivity experiments by a remote sensing process-based terrestrial ecosystem model and a joint-solution method. We found that annual ET increased significantly ($p < 0.05$) with the dominant factor of strong vegetation greening on the national scale. However, despite the significant ($p < 0.05$) increase in precipitation, the water yield throughout vegetated mainland China exhibited an insignificant trend, mainly due to the offsetting effect of vegetation greening (i.e., the enhanced ET). Furthermore, the spatial analyses suggested that vegetation and precipitation dominated the trends in ET over more than half and one-third of the study area, respectively. In contrast, precipitation was the dominant contributor to the trends in water yield over two-thirds of the vegetated mainland China. This highlighted the different mechanisms behind changes in water budgets across vegetated mainland China during the recent two decades. The results could improve our understanding of how climate variables and vegetation dynamics quantitatively caused hydrological changes across vegetated mainland China and could help develop specific measures to maintain water resources availability and regional development. Besides, the finding of this study implied that the spatial differences in the

mechanisms controlling hydrological changes should be considered to maximize ecological and hydrological benefits, when formulating and implementing the ecological recovery policies in China.

Declaration of Competing Interest

The authors declare that they have no known competing financial interests or personal relationships that could have appeared to influence the work reported in this paper.

Data availability

Data will be made available on request.

Acknowledgments

Supplementary materials

Supplementary material associated with this article can be found, in the online version, at doi:10.1016/j.agrformet.2022.109118.

Appendix A. ET computations of the BEPS model

Some main methodologies and recent modifications directly related to the calculation of ET are provided here. In the BEPS model, ET from terrestrial ecosystems is calculated as (Liu, 2003):

$$ET = T_{ran} + E_{plant} + E_{soil} + S_{plant} + S_{ground}, \tag{A1}$$

where T_{ran} is the canopy transpiration; E_{plant} and E_{soil} are the evaporation of intercepted precipitation and soil surface, respectively; S_{plant} and S_{ground} are the snow sublimation from the canopy and ground surface, respectively.

The canopy transpiration is further calculated as:

$$T_{ran} = T_{ran.sunlit}LAI_{sunlit} + T_{ran.shaded}LAI_{shaded}, \tag{A2}$$

where $T_{ran,sunlit}$ and $T_{ran,shaded}$ are the transpiration of the sunlit and shaded leaves, respectively; LAI_{sunlit} and LAI_{shaded} are the LAI of the sunlit and shaded leaves, respectively and they are separated from total LAI according to daily mean solar zenith angle (θ) and clumping index (Ω) (Chen et al., 1999).

The transpiration of sunlit and shaded leaves is calculated using the Penman-Monteith equation (Monteith, 1965):

$$T_{ran.j} = \frac{\Delta R_{n,j} + \rho c_p VPD/r_a}{\left[\Delta + \gamma\left(1 + r_{s,j}/r_a\right)\lambda_v\right]}, \tag{A3}$$

where Δ is the rate of saturated water vapor pressure changing with temperature (kPa °C^{-1}); the subscript j denotes the sunlit or shaded leaves; $R_{n,j}$ is the net radiation (w m^{-2}) absorbed by sunlit or shaded leaves; ρ is the density of air (kg m^{-3}); c_p is the specific heat of the air (J kg^{-1} °C^{-1}); γ is the psychrometric constant (kPa °C^{-1}); r_a is the aerodynamic resistance (s m^{-1}); and $r_{s,j}$ is the stomatal resistance to water vapor (s m^{-1}) of sunlit or shaded leaves.

E_{soil} is also calculated using the Penman-Monteith equation with the resistance of soil surface changing with the degree of saturation within the first soil layer (Ju et al., 2010a, 2010b). E_{plant}, S_{plant}, and S_{ground} are computed in the same way as (Liu et al., 2013).

Appendix B. Soil water content computations of the BEPS model

The BEPS estimates soil water content at three soil profile layers with depths of 0.1 m, 0.25 m, and 0.85 m (Liu et al., 2013). Soil evaporation is limited to the first soil layer. However, vegetation can take water from all three layers through transpiration. Thus, the changes in soil water content at the three soil layers can be expressed as:

$$\frac{\partial \theta_1}{\partial t} = \frac{1}{d_1}\left(P_{gs} - T_{ran,1} - E_{soil} - RF - Q_{1,2}\right), \tag{B1}$$

$$\frac{\partial \theta_2}{\partial t} = \frac{1}{d_2}\left(Q_{1,2} - T_{ran,2} - Q_{2,3}\right), \tag{B2}$$

and

$$\frac{\partial \theta_3}{\partial t} = \frac{1}{d_3} \left(Q_{2,3} - T_{ran,3} - Q_3 \right),$$ (B3)

where θ_i is the water content of soil layer i; d_i is the thickness of soil layer i (m); P_{gs} is precipitation throughfall arriving at the ground surface (m d^{-1}); $T_{ran,i}$ is the transpiration uptake from soil layer i (m d^{-1}); RF is the surface runoff estimated as a function of P_{gs} and θ_1; $Q_{i,i+1}$ is the vertical exchange of soil water between soil layers i and soil layer $i+1$ (m d^{-1}); and Q_3 is the saturated subsurface flow from the bottom of the soil profile and is calculated according to soil water content and saturated hydraulic conductivity in the deepest soil layer.

The soil water flux between layers i and $i+1$ is estimated as (Sellers et al., 1996):

$$Q_{i,i+1} = \frac{k_i d_i + k_{i+1} d_{i+1}}{d_i + d_{i+1}} \left(1 + 2 \frac{w_i - w_{i+1}}{d_i + d_{i+1}} \right),$$ (B4)

where k_i and k_{i+1} are the hydraulic conductivity at soil layers i and $i+1$ (m d^{-1}), respectively; w_i and w_{i+1} are the water potential in soil layers i and $i+1$ (m), respectively.

The hydraulic conductivity (k_i) at soil layer i is calculated as:

$$k_i = K_i \left(\frac{\theta_i}{\theta_{s,i}} \right)^{2b+3},$$ (B5)

where K_i is the saturated hydraulic conductivity of the soil layer (m d^{-1}), and b is a soil texture dependent parameter to determine the changing rate of hydraulic conductivity with soil water content.

Appendix C. Separation algorithm for the joint-solution method

With the assumption that the changed factors induced the EXP$_x$ ET trends, an equation is established as follows:

$$\sum_{K \neq x}^{N} C_{ET}^{K} = T_{ET}^{EXP_x},$$ (C1)

where $\sum_{K \neq i}^{N} C_{ET}^{K}$ represents the sum ET trends contributed from the influential factors (excluding x-factor), N is the number of sensitivity experiments (here being 5), and $T_{ET}^{EXP_x}$ is the linear trend from the EXP$_x$ ET. Thus, we could get a set of simultaneous equations with five unknown numbers (i.e., C_{ET}^{PRE}, C_{ET}^{RAD}, C_{ET}^{T}, C_{ET}^{RH}, and C_{ET}^{VEG}). By solving these equations, the respective contribution for each factor was obtained as follows:

$$C_{ET}^{K} = \frac{\sum_{K \neq i}^{N} T_{ET}^{EXP_K} - (N-2) T_{ET}^{EXP_x}}{(N-1)},$$ (C2)

Appendix D. Identifications of dominant factors for the annual ET and water yield trends

Here is a brief description of the dominant factor for the annual ET and water yield trends on grid cell and regional scales. Firstly, based on the HD-LCC, HD-Cropland, natural vegetation maps (Fig. S1), the contribution of HD-LCC/HD-Cropland/natural vegetation to the ET trends can be identified as vegetation at HD-LCC/HD-Cropland/natural vegetation grid. If the EXP$_{CTL}$ annual ET (water yield) trends are upward, the factor among precipitation, incoming solar radiation, temperature, relative humidity, and HD-LCC/HD-Cropland/natural vegetation with the maximum positive contribution is considered the dominant one. On the other hand, if the EXP$_{CTL}$ annual ET (water yield) trends are downward, the factor with the minimum negative contribution is the dominant factor. Therefore, we first estimate the vegetation contributions to the ET (water yield) trends for a certain region by summing up area-weighted contributions from HD-LCC, HD-Cropland, and natural vegetation. Then, by comparing the contributions of each climate factor and vegetation, the dominants for vegetated mainland China and each water resources region can be determined. Furthermore, if vegetation is dominant for a given region, we further determine the dominant factor to be HD-LCC, HD-Cropland, and natural vegetation based on their contributions.

References

Amthor, J.S., Chen, J.M., Clein, J.S., Frolking, S.E., Goulden, M.L., Grant, R.F., et al., 2001. Boreal forest CO$_2$ exchange and evapotranspiration predicted by nine ecosystem process models: Intermodel comparisons and relationships to field measurements. J. Geophys. Res. Atmos. 106, 33623–33648. https://doi.org/10.1029/2000jd900850.

Bai, P., Liu, X., Zhang, Y., Liu, C., 2020. Assessing the impacts of vegetation greenness change on evapotranspiration and water yield in China. Water Resour. Res. 56, e2019WR027019 https://doi.org/10.1029/2019WR027019.

Brown, A.E., Zhang, L., McMahon, T.A., Western, A.W., Vertessy, R.A., 2005. A review of paired catchment studies for determining changes in water yield resulting from alterations in vegetation. J. Hydrol. 310, 28–61. https://doi.org/10.1016/j.jhydrol.2004.12.010.

Byrne, M.P., O'Gorman, P.A., 2015. The response of precipitation minus evapotranspiration to climate warming: why the "wet-get-wetter, dry-get-drier" scaling does not hold over land. J. Clim. 28, 8078–8092. https://doi.org/10.1175/JCLI-D-15-0369.1.

Cao, S., Chen, L., Shankman, D., Wang, C., Wang, X., Zhang, H., 2011. Excessive reliance on afforestation in China's arid and semi-arid regions: lessons in ecological restoration. Earth Sci. Rev. 104, 240–245. https://doi.org/10.1016/j.earscirev.2010.11.002.

Caldwell, P.V., Kennen, J., Sun, G., Kiang, J., Butcher, J., Eddy, M.C., et al., 2015. A comparison of hydrologic models for ecological flows and water supply. Ecohydrology 8 (8), 1525–1546. https://doi.org/10.1002/eco.1602.

Cavalcante, R.B.L., Pontes, P.R.M., Souza, P.W.M., de Souza, E.B., 2019. Opposite effects of climate and land use changes on the annual water balance in the Amazon arc of

deforestation. Water Resour. Res. 55, 3092–3106. https://doi.org/10.1029/2019WR025083.

Chen, C., Park, T., Wang, X., Piao, S., Xu, B., Chaturved, R.K., et al., 2019a. China and India lead in greening of the world through land-use management. Nat. Sustain. 2, 122–129. https://doi.org/10.1038/s41893-019-0220-7.

Chen, F., Xie, Z., 2010. Effects of interbasin water transfer on regional climate: a case study of the Middle Route of the South-to-North water transfer project in China. J. Geophys. Res. 115, D11112. https://doi.org/10.1029/2009JD012611.

Chen, J.M., Chen, X.Y., Ju, W.M., Geng, X.Y., 2005. Distributed hydrological model for mapping evapotranspiration using remote sensing inputs. J. Hydrol. 305, 15–39. https://doi.org/10.1016/j.jhydrol.2004.08.029.

Chen, J.M., Deng, F., Chen, M., 2006. Locally adjusted cubic-spline capping for reconstructing seasonal trajectories of a satellite-derived surface parameter. IEEE Trans. Geosci. Remote Sens. 44 (8), 2230–2238. https://doi.org/10.1109/TGRS.2006.872089.

Chen, J.M., Ju, W.M., Ciais, P., Viovy, N., Liu, R.G., Liu, Y., et al., 2019b. Vegetation structural change since 1981 significantly enhanced the terrestrial carbon sink. Nat. Commun. 10, 4259. https://doi.org/10.1038/s41467-019-12257-8.

Chen, J.M., Liu, J., Cihlar, J., Goulden, M.L., 1999. Daily canopy photosynthesis model through temporal and spatial scaling for remote sensing applications. Ecol. Model. 124, 99–119. https://doi.org/10.1016/S0304-3800(99)00156-8.

Chen, L., Dirmeyer, P.A., 2018. Global observed and modelled impacts of irrigation on surface temperature. Int. J. Climatol. 39 (5), 2587–2600. https://doi.org/10.1002/joc.5973.

Chen, S., Chen, J., Lin, G., Zhang, W., Miao, H., Wei, L., et al., 2009. Energy balance and partition in Inner Mongolia steppe ecosystems with different land use types. Agric. For. Meteorol. 149 (11), 1800–1809. https://doi.org/10.1016/j.agrformet.2009.06.009.

Chen, Y., Feng, X., Tian, H., Wu, X., Gan, Z., Feng, Y., et al., 2021. The contributions of climate change and human activities on vegetation carbon sequestration in China during 2001–2018. Glob. Chang. Biol. 27 (22), 5848–5864. https://doi.org/10.1111/gcb.15854.

Chen, Y., Wang, K., Lin, Y., Shi, W., Song, Y., He, X., 2015. Balancing green and grain trade. Nat. Geosci. 8, 739–741. https://doi.org/10.1038/ngeo2544.

Cortés, J., Mahecha, M.D., Reichstein, M., Myneni, R.B., Chen, C., Brenning, A, 2021. Where are global vegetation greening and browning trends significant? Geophys. Res. Lett. 48 (6), e2020GL091496 https://doi.org/10.1029/2020GL091496.

Damour, G., Simonneau, T., Cochard, H., Urban, L., 2010. An overview of models of stomatal conductance at the leaf level. Plant Cell Environ. 33 (9), 1419–1438. https://doi.org/10.1111/j.1365-3040.2010.02181.x.

Deng, F., Chen, J.M., Plummer, S., Chen, M.Z., Pisek, J., 2006. Algorithm for global leaf area index retrieval using satellite imagery. IEEE Trans. Geosci. Remote Sens. 44 (8), 2219–2229. https://doi.org/10.1109/TGRS.2006.872100.

Droogers, P., Immerzeel, W.W., Lorite, I.J., 2010. Estimating actual irrigation application by remotely sensed evapotranspiration observations. Agric. Water Manag. 97 (9), 1351–1359. https://doi.org/10.1016/j.agwat.2010.03.017.

Ellison, D., Futter, M.N., Bishop, K., 2012. On the forest cover-water yield debate: from demand-to supply-side thinking. Glob. Chang. Biol. 18, 806–820. https://doi.org/10.1111/j.1365-2486.2011.02589.

Fang, H., Baret, F., Plummer, S., Schaepman-Strub, G., 2019. An overview of global leaf area index (LAI): Methods, products, validation, and applications. Rev. Geophys. 57 (3), 739–799. https://doi.org/10.1029/2018RG000608.

Feng, D., Fu, M., Sun, Y., Bao, W., Zhang, M., Zhang, Y., et al., 2021a. How large-scale anthropogenic activities influence vegetation cover change in China? A review. Forests 12 (3), 320. https://doi.org/10.3390/f12030320.

Feng, X., Fu, B., Piao, S., Wang, S., Ciais, P., Zeng, Z., et al., 2016. Revegetation in China's Loess Plateau is approaching sustainable water resource limits. Nat. Clim. Chang. 6 (11), 1019–1022. https://doi.org/10.1038/nclimate3092.

Feng, X., Fu, B., Zhang, Y., Pan, N., Peuelas, J., 2021b. Recent leveling off of vegetation greenness and primary production reveals the increasing soil water limitations on the greening Earth. Sci. Bull. 66 (14), 1462–1471. https://doi.org/10.1016/j.scib.2021.02.023.

Feng, X., Liu, G., Chen, J.M., Chen, M., Liu, J., Ju, W.M., et al., 2007. Net primary productivity of China's terrestrial ecosystems from a process model driven by remote sensing. J. Environ. Manag. 85, 563–573. https://doi.org/10.1016/j.jenvman.2006.09.021.

Fernandes, R., Korolevych, V., Wang, S., 2009. Trends in land evapotranspiration over Canada for the period 1960–2000 based on *in situ* climate observations and a land surface model. J. Hydrometeorol. 8 (5), 1016–1030. https://doi.org/10.1175/JHM619.1.

Friedl, M.A., Sulla-Menashe, D., Tan, B., Schneider, A., Ramankutty, N., Sibley, A., et al., 2010. MODIS Collection 5 global land cover: algorithm refinements and characterization of new datasets. Remote Sens. Environ. 114 (1), 68–182. https://doi.org/10.1016/j.rse.2009.08.016.

Fu, X., Yu, G., Sun, X., Li, Y., Wen, X., Zhang, L., et al., 2006. Depression of net ecosystem CO_2 exchange in semi-arid Leymus chinensis steppe and alpine shrub. Agric. For. Meteorol. 137, 234–244. https://doi.org/10.1016/j.agrformet.2006.02.009.

Galleguillos, M., Jacob, F., Prevot, L., French, A., Lagacherie, P., 2011. Comparison of two temperature differencing methods to estimate daily evapotranspiration over a Mediterranean vineyard watershed from ASTER data. Remote Sens. Environ. 115 (6), 1326–1340. https://doi.org/10.1016/j.rse.2011.01.013.

Gao, Y., Lv, S., Cheng, G., 2003. Simulation of rainfall-runoff and watershed convergence process in the upper reaches of Heihe River Basin, July 2002. Sci. China Ser. D Earth Sci. 47 (S1), 1–8. https://doi.org/10.1360/04zd0001.

Gao, Y., Pu, S., Zheng, C., Yi, S., 2019b. An improved method for the calculation of unsaturated–saturated water flow by coupling the FEM and FDM. Sci. Rep. 9, 14995. https://doi.org/10.1038/s41598-019-51405-4.

Gedney, N., Cox, P.M., Betts, R.A., Boucher, O., Huntingford, C., Stott, P.A., 2006. Detection of a direct carbon dioxide effect in continental river runoff records. Nature 439 (7078), 835–838. https://doi.org/10.1038/nature04504.

Gray, S.B., Brady, S.M., 2016. Plant developmental responses to climate change. Dev. Biol. 419, 64–77. https://doi.org/10.1016/j.ydbio.2016.07.023.

Govind, A., Chen, J., McDonnell, J., Kumari, J., Sonnentag, O., 2011. Effects of lateral hydrological processes on photosynthesis and evapotranspiration in a boreal ecosystem. Ecohydrology 4 (3), 394–410. https://doi.org/10.1002/eco.141.

Greve, P., Gudmundsson, L., Seneviratne, S.I., 2018. Regional scaling of annual mean precipitation and water availability with global temperature change. Earth Syst. Dyn. 9, 227–240. https://doi.org/10.5194/esd-2017-62.

Greve, P., Seneviratne, S.I., 2015. Assessment of future changes in water availability and aridity. Geophys. Res. Lett. 42, 5493–5499. https://doi.org/10.1002/2015GL064127.

Guan, D., Wu, J., Zhao, X., Han, S., Yu, G., Sun, X., et al., 2006. CO_2 flux over old temperate mixed forest in North-eastern China. Agric. For. Meteorol. 137, 138–149. https://doi.org/10.1016/j.agrformet.2006.02.00310.1016/j.agrformet.2006.02.003.

Gupta, H.V., Kling, H., Yilmaz, K.K., Martinez, G.F., 2012. Decomposition of the mean squared error and NSE performance criteria: implications for improving hydrological modelling. J. Hydrol. 377, 80–91. https://doi.org/10.1016/j.jhydrol.2009.08.003.

Han, S., Hu, H., Yang, D., Liu, Q., 2011. Irrigation impact on annual water balance of the oases in Tarim Basin, Northwest China. Hydrol. Process. 25, 167–174. https://doi.org/10.1002/hyp.7830.

He, L., Chen, J.M., Pisek, J., Schaaf, C.B., Strahler, A.H., 2012. Global clumping index map derived from the MODIS BRDF product. Remote Sens. Environ. 119, 118–130. https://doi.org/10.1016/j.rse.2011.12.008.

He, Q., Ju, W.M., Dai, S.P., He, W., Song, L., Wang, S.H., et al., 2021. Drought risk of global terrestrial gross primary productivity over the last 40 years detected by a remote sensing-driven process model. J. Geophys. Res. Biogeosci. 117, G01023. https://doi.org/10.1029/2020JG005944.

Hersbach, H., Bell, B., Berrisford, P., Hirahara, S., Horányi, A., Muñoz-Sabater, J., et al., 2020. The ERA5 global reanalysis. Q. J. R. Meteorol. Soc. 146, 1999–2049. https://doi.org/10.1002/qj.3803.

Hiyama, A., Takemiya, A., Munemasa, S., Okuma, E., Sugiyama, N., Tada, Y., et al., 2017. Blue light and CO_2 signals converge to regulate light-induced stomatal opening. Nat. Commun. 8, 1–13. https://doi.org/10.1038/s41467-017-01237-5.

Jarvis, P.G., 1976. The interpretation of the variations in leaf water potential and stomatal conductance found in canopies in the field. Philos. Trans. R Soc. Lond. B 273, 593–610. https://doi.org/10.1098/rstb.1976.0035.

Jansson, P., Hock, R., Schneider, T., 2003. The concept of glacier storage: a review. J. Hydrol. 282, 116–129. https://doi.org/10.1016/S0022-1694(03)00258-0.

Jiang, C., Ryu, Y., Fang, H., Myneni, R., Claverie, M., Zhu, Z., 2017. Inconsistencies of interannual variability and trends in long-term satellite leaf area index products. Glob. Chang. Biol. 23 (10), 4133–4146. https://doi.org/10.1111/gcb.13787.

Jong, R.D., Verbesselt, J., Schaepman, M.E., Bruin, S.D., 2012. Trend changes in global greening and browning: contribution of short-term trends to longer-term change. Glob. Chang. Biol. 18 (2), 642–655. https://doi.org/10.1111/j.1365-2486.2011.02578.x.

Ju, W.M., Chen, J.M., Black, T.A., Barr, A.G., Liu, J., Chen, B., et al., 2006. Modelling multi-year coupled carbon and water fluxes in a boreal aspen forest. Agric. For. Meteorol. 140, 136–151. https://doi.org/10.1016/j.agrformet.2006.08.008.

Ju, W.M., Gao, P., Zhou, Y.L., Chen, J.M., Chen, S., Li, X.F., 2010a. Prediction of summer grain crop yield with a process-based ecosystem model and remote sensing data for the northern area of the Jiangsu Province, China. Int. J. Remote Sens. 31, 1573–1587. https://doi.org/10.1080/01431160903475357.

Ju, W., Gao, P., Wang, J., Zhou, Y., Zhang, X., 2010b. Combining an ecological model with remote sensing and GIS techniques to monitor soil water content of croplands with a monsoon climate. Agric. Water Manag. 97, 1221–1231. https://doi.org/10.1016/j.agwat.2009.12.007.

Katul, G.G., Oren, R., Manzoni, S., Higgins, C., Parlange, M.B., 2012. Evapotranspiration: A process driving mass transport and energy exchange in the soil-plant-atmosphere-climate system. Rev. Geophys. 50, RG3002. https://doi.org/10.1029/2011RG000366.

Kumar, S., Lawrence, D.M., Dirmeyer, P.A., Sheffield, J., 2014. Less reliable water availability in the 21st century climate projections. Earth's Future 2 (3), 152–160. https://doi.org/10.1002/2013ef000159.

Lei, H., Yang, D., Yang, H., Yuan, Z., Lv, H., 2014. Simulated impacts of irrigation on evapotranspiration in a strongly exploited region: a case study of the Haihe River basin, China. Hydrol. Process. 29 (12), 2704–2719. https://doi.org/10.1002/hyp.10402.

Lhomme, J.P., 2001. Stomatal control of transpiration: Examination of the Jarvis-type representation of canopy resistance in relation to humidity. Water Resour. Res. 37 (3), 689–699. https://doi.org/10.1029/2000WR900324.

Li, Q.Q., Chen, Y.H., Liu, M.Y., Zhou, X.B., Dong, B.D., Yu, S.L., 2007. Effect of irrigation to winter wheat on the soil moisture, evapotranspiration, and water use efficiency of summer maize in North China. Trans. ASABE 50 (6), 2073–2080. https://doi.org/10.13031/2013.24109.

Li, X., Cheng, G., Ge, Y., Li, H., Han, F., Tian, W., et al., 2018. Hydrological cycle in the Heihe River Basin and its implication for water resource management in endorheic basins. J. Geophys. Res. Atmos. 123, 890–914. https://doi.org/10.1002/2017JD027889.

Li, X., Cheng, G., Liu, S., Xiao, Q., Ma, M., Jin, R., et al., 2013. Heihe watershed allied telemetry experimental research (HiWATER): scientific objectives and experimental design. Bull. Am. Meteorol. Soc. 94 (8), 1145–1160. https://doi.org/10.1175/BAMS-D-12-00154.1.

Li, X., Liu, S., Xiao, Q., Ma, M., Jin, R., Che, T., et al., 2017. A multiscale dataset for understanding complex eco-hydrological processes in a heterogeneous oasis system. Sci. Data 4, 170083. https://doi.org/10.1038/sdata.2017.83.

Li, X., Yang, K., Zhou, Y., 2016. Progress in the study of oasis-desert interactions. Agric. For. Meteorol. 230–231, 1–7. https://doi.org/10.1016/j.agrformet.2016.08.022.

Li, Y., Sun, X., Zhao, X., Zhao, L., Xu, S., Gu, S., et al., 2006. Seasonal variations and mechanism for environmental control of NEE concerning the Potentilla Fruticosa in alpine shrub meadow of Qinghai-Tibet Plateau. Sci. China Ser. D Earth Sci. 49 (S2), 174–185. https://doi.org/10.1007/s11430-006-8174-9.

Li, Z., Quiring, S.M., 2021. Identifying the dominant drivers of hydrological change in the contiguous United States. Water Resour. Res. 57 (5), e2021WR029738 https://doi.org/10.1029/2021WR029738.

Lian, X., Piao, S., Li, L.Z.X., Li, Y., Huntingford, C., Ciais, P., et al., 2020. Summer soil drying exacerbated by earlier spring greening of northern vegetation. Sci. Adv. 6 (1), eaax0255. https://doi.org/10.1126/sciadv.aax0255.

Lin, S., Wang, G., Hu, Z., Huang, K., Sun, X., Sun, J., et al., 2021. Dynamics of evapotranspiration and variations in different land-cover regions over the Tibetan Plateau during 1961–2014. J. Hydrometeorol. 22 (4), 955–969. https://doi.org/10.1175/JHM-D-20-0074.1.

Liu, J., Chen, J.M., Cihlar, J., 2003. Mapping evapotranspiration based on remote sensing: an application to Canada's landmass. Water Resour. Res. 39, 1189. https://doi.org/10.1029/2002WR001680.

Liu, Q., McVicar, T.R., Yang, Z., Donohue, R.J., Liang, L., Yang, Y., 2016a. The hydrological effects of varying vegetation characteristics in a temperate water-limited basin: development of the dynamic Budyko-Choudhury-Porporato (dBCP) model. J. Hydrol. 543, 595–611. https://doi.org/10.1016/j.jhydrol.2016.10.035.

Liu, R., Liu, Y., 2013. Generation of new cloud masks from MODIS land surface reflectance products. Remote Sens. Environ. 133, 21–37. https://doi.org/10.1016/j.rse.2013.01.019.

Liu, S., Xu, Z., Wang, W., Bai, J., Jia, Z., Zhu, M., et al., 2011. A comparison of eddy-covariance and large aperture scintillometer measurements with respect to the energy balance closure problem. Hydrol. Earth Syst. Sci. 15 (4), 1291–1306. https://doi.org/10.5194/hess-15-1291-2011.

Liu, W., Wei, X., Liu, S., Liu, Y., Fan, H., Zhang, M., et al., 2015a. How do climate and forest changes affect long-term streamflow dynamics? A case study in the upper reach of Poyang River basin. Ecohydrology 8 (1), 46–57. https://doi.org/10.1002/eco.1486.

Liu, Y., Liu, R., Chen, J.M., 2012. Retrospective retrieval of long-term consistent global leaf area index (1981–2011) from combined AVHRR and MODIS data. J. Geophys. Res. Biogeosci. 117 (G4) https://doi.org/10.1029/2012jg002084.

Liu, Y., Xiao, J., Ju, W., Xu, K., Zhou, Y., Zhao, Y., 2016b. Recent trends in vegetation greenness in China significantly altered annual evapotranspiration and water yield. Environ. Res. Lett. 11, 094010 https://doi.org/10.1088/1748-9326/11/9/094010.

Liu, Y., Xiao, J., Ju, W., Zhou, Y., Wang, S., Wu, X., 2015b. Water use efficiency of China's terrestrial ecosystems and responses to drought. Sci. Rep. 5, 13799. https://doi.org/10.1038/srep13799.

Liu, Y., Xiao, J., Ju, W., Zhu, G., Wu, X., Fan, W., 2018. Satellite-derived LAI products exhibit large discrepancies and can lead to substantial uncertainty in simulated carbon and water fluxes. Remote Sens. Environ. 206, 174–188. https://doi.org/10.1016/j.rse.2017.12.024.

Liu, Y., Zhou, Y., Ju, W., Chen, J., Wang, S., He, H., et al., 2013. Evapotranspiration and water yield over China's landmass from 2000 to 2010. Hydrol. Earth Syst. Sci. 17 (12), 4957–4980. https://doi.org/10.5194/hess-17-4957-2013.

Luo, X.Z., Chen, J.M., Liu, J., Black, T.A., Croft, H., Staebler, R., et al., 2018. Comparison of big-leaf, two-big-leaf, and two-leaf upscaling schemes for evapotranspiration estimation using coupled carbon-water modeling. J. Geophys. Res. Biogeosci. 123, 207–225. https://doi.org/10.1002/2017JG003978.

Ma, N., Zhang, Y., 2022. Increasing Tibetan Plateau terrestrial evapotranspiration primarily driven by precipitation. Agric. For. Meteorol. 317, 108887 https://doi.org/10.1016/j.agrformet.2022.108887.

Mao, J., Shi, X., Thornton, P.E., Hoffman, F.M., Zhu, Z., Myneni, R.B., 2013. Global latitudinal-asymmetric vegetation growth trends and their driving mechanisms: 1982–2009. Remote Sensing 5 (3), 1484–1490. https://doi.org/10.3390/rs5031484.

Mao, Y., Wang, K., Liu, X., Liu, C., 2016. Water storage in reservoirs built from 1997 to 2014 significantly altered the calculated evapotranspiration trends over China. J. Geophys. Res. Atmos. 121, 10097–10112. https://doi.org/10.1002/2016JD025447.

Marshall, M, Funk, C., Michaelsen, J., 2012. Examining evapotranspiration trends in Africa. Clim. Dyn. 38, 1849–1865. https://doi.org/10.1007/s00382-012-1299-y.

Martens, B., Miralles, D.G., Lievens, H., van der Schalie, R., de Jeu, R.A.M., Fernández-Prieto, D., et al., 2017. GLEAM v3: satellite-based land evaporation and root-zone soil moisture. Geosci. Model Dev. 10, 1903–1925. https://doi.org/10.5194/gmd-10-1903-2017.

Matsushita, B., Tamura, M., 2002. Integrating remotely sensed data with an ecosystem model to estimate net primary productivity in East Asia. Remote Sens. Environ. 81, 58–66. https://doi.org/10.1016/S0034-4257(01)00331-5.

Meng, S., Xie, X., Zhu, B., Wang, Y., 2020. The relative contribution of vegetation greening to the hydrological cycle in the Three-North region of China: a modelling analysis. J. Hydrol. 591, 125689 https://doi.org/10.1016/j.jhydrol.2020.125689.

Merbold, L., Kutsch, W.L., Corradi, C., Kolle, O., Rebmann, C., Stoy, P.C., et al., 2009. Artificial drainage and associated carbon fluxes (CO_2/CH_4) in a tundra ecosystem.

Glob. Chang. Biol. 15 (11), 2599–2614. https://doi.org/10.1111/j.1365-2486.2009.01962.x.

Milly, P.C., Dunne, K.A., Vecchia, A.V., 2005. Global pattern of trends in streamflow and water availability in a changing climate. Nature 438, 347–350. https://doi.org/10.1038/nature04312.

Miralles, D.G., Holmes, T.R.H., de Jeu, R.A.M., Gash, J.H., Meesters, A.G.C.A., Dolman, A.J., 2011. Global land-surface evaporation estimated from satellite-based observations. Hydrol. Earth Syst. Sci. 15, 453–469. https://doi.org/10.5194/hess-15-453-2011.

Molod, A., Takacs, L., Suarez, M., Bacmeister, J., 2015. Development of the GEOS-5 atmospheric general circulation model: evolution from MERRA to MERRA-2. Geosci. Model Dev. 8, 1339–1356.

Monteith, J.L., 1965. Evaporation and environment. In: Fogg, G.E. (Ed.), The State and Movement of Water in Living Organisms. Cambridge University Press, Cambridge.

Muñoz-Sabater, J. (2019). ERA5-Land monthly averaged data from 1981 to present. Copernicus Climate Change Service (C3S) Climate Data Store (CDS). (Accessed on: 20-04-2022). 10.24381/cds.68d2bb30.

Mu, Q., Heinsch, F.A., Zhao, M., Running, S.W., 2007. Development of a global evapotranspiration algorithm based on MODIS and global meteorology data. Remote Sens. Environ. 111, 519–536. https://doi.org/10.1016/j.rse.2007.04.015.

Norby, R.J., Delucia, E.H., Gielen, B., Calfapietra, C., Giardina, C.P., et al., 2005. Forest response to elevated CO_2 is conserved across a broad range of productivity. Proc. Natl. Acad. Sci. U.S. 102 (50), 18052–18056. https://doi.org/10.1073/pnas.0509478102.

Odongo, V.O., Oel, P.R., der Tol, C., Su, Z., 2019. Impact of land use and land cover transitions and climate on evapotranspiration in the Lake Naivasha Basin, Kenya. Sci. Total Environ. 682, 19–30. https://doi.org/10.1016/j.scitotenv.2019.04.062.

Papagiannopoulou, C., Miralles, D., Dorigo, W.A., Verhoest, N.E.C., Depoorter, M., Waegeman, W., 2017. Vegetation anomalies caused by antecedent precipitation in most of the world. Environ. Res. Lett. 12, 074016 https://doi.org/10.1088/1748-9326/aa7145.

Piao, S., Wang, X., Park, T., Chen, C., Lian, X., He, Y., et al., 2020. Characteristics, drivers and feedbacks of global greening. Nat. Rev. Earth Environ. 1, 14–27. https://doi.org/10.1038/s43017-019-0001-x.

Piao, S., Yin, G., Tan, J., Cheng, L., Huang, M., Li, Y., et al., 2015. Detection and attribution of vegetation greening trend in China over the last 30 years. Glob. Chang. Biol. 21 (4), 1601–1609. https://doi.org/10.1111/gcb.12795.

Pielke, R.A., 2005. Land use and climate change. Science 310 (5754), 1625–1626. https://doi.org/10.1126/science.1120529.

Potter, N.J., Zhang, L., Milly, P.C.D., McMahon, T.A., Jakeman, A.J., 2005. Effects of rainfall seasonality and soil moisture capacity on mean annual water balance for Australian catchments. Water Resour. Res. 41 (6), W06007. https://doi.org/10.1029/2004WR003697.

Qu, S., Wang, L., Lin, A., Zhu, H., Yuan, M., 2018. What drives the vegetation restoration in Yangtze River basin, China: climate change or anthropogenic factors? Ecol. Indic. 90, 438–450. https://doi.org/10.1016/j.ecolind.2018.03.029.

Reichle, R.H., Koster, R.D., de Lannoy, G.J.M., Forman, B.A., Liu, Q., Mahanama, S.P.P., et al., 2011. Assessment and enhancement of MERRA land surface hydrology estimates. J. Clim. 24, 6322–6338. https://doi.org/10.1175/jcli-d-10-05033.1.

Reichstein, M., Falge, E., Baldocchi, D., Papale, D., Aubinet, M., Berbigier, P., et al., 2005. On the separation of net ecosystem exchange into assimilation and ecosystem respiration: Review and improved algorithm. Glob. Chang. Biol. 11, 1424–1439. https://doi.org/10.1111/j.1365-2486.2005.001002.x.

Ribes, A., Decharme, B., Alkama, R., Sheffield, J., 2013. Anthropogenic influence on multidecadal changes in reconstructed global evapotranspiration. Nat. Clim. Chang. 3 (1), 59–62. https://doi.org/10.1038/nclimate1632.

Rodell, M., Houser, P.R., Jambor, U., Gottschalck, J., Mitchell, K., Meng, C.-J., et al., 2004. The global land data assimilation system. Bull. Am. Meteorol. Soc. 85, 381–394. https://doi.org/10.1007/978-94-010-0029-1_30.

Rohatyn, S., Rotenberg, E., Ramati, E., Tatarinov, F., Tas, E., Yakir, D., 2018. Differential impacts of land use and precipitation on "ecosystem water yield. Water Resour. Res. 54, 5457–5470. https://doi.org/10.1029/2017WR022267.

Ruiz-Péreza, G., González-Sanchis, M., Del Campo, A.D., Francésa, F., 2016. Can a parsimonious model implemented with satellite data be used for modelling the vegetation dynamics and water cycle in water-controlled environments? Ecol. Model. 324, 45–53. https://doi.org/10.1016/j.ecolmodel.2016.01.002.

Rummler, T., Arnault, J., Gochis, D., Kunstmann, H., 2019. Role of lateral terrestrial water flow on the regional water cycle in a complex terrain region: Investigation with a fully coupled model system. J. Geophys. Res. Atmos. 124, 507–529. https://doi.org/10.1029/2018JD029004.

Running, S., Mu, Q., & Zhao, M. (2017). MOD16A2 MODIS/Terra Net Evapotranspiration 8-Day L4 Global 500m SIN Grid V006. NASA EOSDIS Land Processes DAAC. 10.5067/MODIS/MOD16A2.006.

Running, S.W., Coughlan, J.C., 1988. A general model of forest ecosystem processes for regional applications I. Hydrologic balance, canopy gas exchange and primary production processes. Ecol. Model. 42 (2), 125–154. https://doi.org/10.1016/0304-3800(88)90112-3.

Ruscica, R.C., Sörensson, A.A., Diaz, L.B., Vera, C., Castro, A., Papastefanou, P., et al., 2021. Evapotranspiration trends and variability in southeastern South America: The roles of land-cover change and precipitation variability. Int. J. Climatol. https://doi.org/10.1002/joc.7350.

Schwalm, C.R., Williams, C.A., Schaefer, K., Anderson, R., Arain, M.A., Barr, A., et al., 2010. A model-data intercomparison of CO_2 exchange across North America: results from the North American Carbon Program site synthesis. J. Geophys. Res. Biogeosci. 115, G00H05. https://doi.org/10.1029/2009JG001229.

Seager, R., Ting, M., Li, C., Naik, N., Cook, B., Nakamura, J., et al., 2013. Projections of declining surface-water availability for the southwestern United States. Nat. Clim. Chang. 3, 482–486. https://doi.org/10.1038/nclimate1787.

Sellers, P.J., Randall, D.A., Collatz, G.J., Berry, J.A., Field, C.B., Dazlich, D.A., et al., 1996. A revised land surface parameterization (SiB2) for atmospheric GCMs. Part I: model formulation. J. Clim. 9 (4), 676–705. https://doi.org/10.1175/1520-0442 (1996)009<0676:ARLSPF>2.0.CO;2.

Senatore, A., Mendicino, G., Gochis, D.J., Yu, W., Yates, D.N., Kunstmann, H., 2015. Fully coupled atmospherehydrology simulations for the central Mediterranean: Impact of enhanced hydrological parameterization for short and long time scales. J. Adv. Model. Earth Syst. 7, 1693–1715. https://doi.org/10.1002/2015MS000510.

Seneviratne, S.I., Lüthi, D., Litschi, M., Schär, C., 2006. Land–atmosphere coupling and climate change in Europe. Nature 443 (7108), 205–209. https://doi.org/10.1038/nature05095.

Shangguan, W., Dai, Y., Liu, B., Ye, A., Yuan, H., 2012. A soil particle-size distribution dataset for regional land and climate modelling in China. Geoderma 171–172, 85–91. https://doi.org/10.1016/j.geoderma.2011.01.013.

Sheil, D., Murdiyarso, D., 2009. How forests attract rain: an examination of a new hypothesis. Bioscience 59, 341–347. https://doi.org/10.1525/bio.2009.59.4.12.

Shen, Y., Zhang, Y., Scanlon, B.R., Lei, H., Yang, D., Yang, F., 2013. Energy/water budgets and productivity of the typical croplands irrigated with groundwater and surface water in the North China Plain. Agric. For. Meteorol. 181, 133–142. https://doi.org/10.1016/j.agrformet.2013.07.013.

Sonnentag, O., Chen, J.M., Roulet, N.T., Ju, W., Govind, A., 2008. Spatially explicit simulation of peatland hydrology and carbon dioxide exchange: Influence of mesoscale topography. J. Geophys. Res. Biogeosci. 113, G02005. https://doi.org/10.1029/2007JG000605.

Sprintsin, M., Chen, J.M., Desai, A., Gough, C.M., 2012. Evaluation of leaf-to-canopy upscaling methodologies against carbon flux data in North America. J. Geophys. Res. Biogeosci. 117, G01023. https://doi.org/10.1029/2010jg001407.

Sulla-Menashe, D., Gray, J.M., Abercrombie, S.P., Friedl, M.A., 2019. Hierarchical mapping of annual global land cover 2001 to present: the MODIS collection 6 land cover product. Remote Sens. Environ. 222, 183–194. https://doi.org/10.1016/j.rse.2018.12.013.

Sun, G., Caldwell, P.V., McNulty, S.G., 2015. Modelling the potential role of forest thinning in maintaining water supplies under a changing climate across the conterminous United States. Hydrol. Process. 29, 5016–5030. https://doi.org/10.1002/hyp.10469.

Sun, G., Zhou, G., Zhang, Z., Wei, X., McNulty, S.G., Vose, J.M., 2006a. Potential water yield reduction due to forestation across China. J. Hydrol. 328 (3–4), 548–558. https://doi.org/10.1016/j.jhydrol.2005.12.013.

Sun, S., Bi, Z., Zhou, S., Wang, H., Li, Q., Liu, Y., Wang, G., et al., 2021. Spatiotemporal shifts in key hydrological variables and dominant factors over China. Hydrol. Process. 35, e14319. https://doi.org/10.1002/hyp.14319.

Sun, S., Chen, H., Ju, W., Song, J., Zhang, H., Sun, J., et al., 2013. Effects of climate change on annual streamflow using climate elasticity in Poyang Lake Basin, China. Theor. Appl. Climatol. 112, 169–183. https://doi.org/10.1007/s00704-012-0714-y.

Sun, S., Chen, H., Ju, W., Yu, M., Hua, W., Yin, Y., 2014. On the attribution of the changing hydrological cycle in Poyang Lake Basin, China. J. Hydrol. 514, 214–225. https://doi.org/10.1016/j.jhydrol.2014.04.013.

Sun, S., Chen, H., Sun, G., Ju, W., Wang, G., Li, X., et al., 2017. Attributing the changes in reference evapotranspiration in Southwestern China using a new separation method. J. Hydrometeorol. 18, 777–798. https://doi.org/10.1175/JHM-D-16-0118.1.

Sun, S., Shi, W., Zhou, S., Chai, R., Chen, H., Wang, G., et al., 2020. Capacity of satellite-based and reanalysis precipitation products in detecting long-term trends across Mainland China. Remote Sens. 12, 2902. https://doi.org/10.3390/rs12182902.

Sun, X., Zhu, Z., Wen, X., Yuan, G., Yu, G, 2006b. The impact of averaging periods on eddy fluxes observed at ChinaFLUX sites. Agric. For. Meteorol. 137, 188–193. https://doi.org/10.1016/j.agrformet.2006.02.012.

Tao, S.L., Fang, J.Y., Ma, S.H., Cai, Q., Xiong, X.Y., Tian, D., et al., 2020. Changes in China's lakes: climate and human impacts. Natl. Sci. Rev. 7, 132–140. https://doi.org/10.1093/nsr/nwz103.

Teuling, A.J., de Badts, E.A.G., Jansen, F.A., Fuchs, R., Buitink, J., van Dijke, A.J.H., et al., 2019. Climate change, reforestation/afforestation, and urbanization impacts on evapotranspiration and streamflow in Europe. Hydrol. Earth Syst. Sci. 23, 3631–3652. https://doi.org/10.5194/hess-23-3631-2019.

Teuling, A.J., Van Loon, A.F., Seneviratne, S.I., Lehner, I., Aubinet, M., Heinesch, B., et al., 2013. Evapotranspiration amplifies European summer drought. Geophys. Res. Lett. 40, 2071–2075. https://doi.org/10.1002/grl.50495.

Tian, F., Lü, Y.H., Fu, B.J., Zhang, L., Zang, C.F., Yang, Y.H., et al., 2017. Challenge of vegetation greening on water resources sustainability: insights from a modeling-based analysis in Northwest China. Hydrol. Process. 31 (7), 1469–1478. https://doi.org/10.1002/hyp.11118.

Vuichard, N., Papale, D., 2015. Filling the gaps in meteorological continuous data measured at FLUXNET sites with ERA-Interim reanalysis. Earth Syst. Sci. Data 7, 157–171. https://doi.org/10.5194/essd-7-157-2015.

Vörösmarty, C.J., Sahagian, D., 2000. Anthropogenic disturbance of the terrestrial water cycle. Bioscience 50 (9), 753–765. https://doi.org/10.1641/0006-3568(2000)050 [0753:ADOTTW]2.0.CO;2.

Wang, D.L., Feng, H.M., Zhang, B.Z., Wei, Z., Tian, Y.L., 2021. Quantifying the impacts of climate change and vegetation change on decreased runoff in China's Yellow River basin. Ecohydrol. Hydrobiol. https://doi.org/10.1016/j.ecohyd.2021.10.002.

Wang, H., Guan, H., Liu, N., Soulsby, C., Tetzlaff, D., Zhang, X., 2020. Improving the Jarvis-type model with modified temperature and radiation functions for sap flow simulations. J. Hydrol. 587, 124981 https://doi.org/10.1016/j.jhydrol.2020.124981.

Wang, H., Li, X., Xiao, J., Ma, M., 2021. Evapotranspiration components and water use efficiency from desert to alpine ecosystems in drylands. Agric. For. Meteorol. 298–299, 108283 https://doi.org/10.1016/j.agrformet.2020.108283.

Wang, K., Dickinson, R.E., 2012. A review of global terrestrial evapotranspiration: observation, modeling, climatology, and climatic variability. Rev. Geophys. 50 (2), RG2005. https://doi.org/10.1029/2011RG000373.

Wang, L., Jia, B., Xie, Z., Wang, B., Liu, S., Li, R., et al., 2022. Impact of groundwater extraction on hydrological process over the Beijing-Tianjin-Hebei region, China. J. Hydrol. 609, 127689 https://doi.org/10.1016/j.jhydrol.2022.127689.

Wang, Q., Tenhunen, J., Falge, E., Bernhofer, C., Granier, A., Vesala, T., 2004. Simulation and scaling of temporal variation in gross primary production for coniferous and deciduous temperate forests. Glob. Chang. Biol. 10, 37–51. https://doi.org/10.1111/j.1365-2486.2003.00716.x.

Wen, X., Yu, G., Sun, X., Li, Q., Liu, Y., Zhang, L., et al., 2005. Soil moisture effects on the temperature dependence of ecosystem respiration in a subtropical Pinus plantation of southern China. Agric. For. Meteorol. 137, 166–175. https://doi.org/10.1016/j.agrformet.2006.02.005.

Williams, C.A., Reichstein, M., Buchmann, N., Baldocchi, D., Beer, C., Schwalm, C., et al., 2012. Climate and vegetation controls on the surface water balance: synthesis of evapotranspiration measured across a global network of flux towers. Water Resour. Res. 48, W06523. https://doi.org/10.1029/2011WR011586.

Xiao, J.F., 2014. Satellite evidence for significant biophysical consequences of the 'grain for green' program on the Loess Plateau in China. J. Geophys. Res. Biogeosci. 119, 2261–2275. https://doi.org/10.1002/2014JG002820.

Xie, S., Mo, X., Hu, S., Liu, S., 2020. Contributions of climate change, elevated atmospheric CO_2 and human activities to ET and GPP trends in the Three-North Region of China. Agric. For. Meteorol. 295, 108183 https://doi.org/10.1016/j.agrformet.2020.108183.

Xie, X., He, B., Guo, L., Miao, C., Zhang, Y., 2019. Detecting hotspots of interactions between vegetation greenness and terrestrial water storage using satellite observations. Remote Sens. Environ. 231, 111259 https://doi.org/10.1016/j.rse.2019.111259.

Xu, M., Kang, S., Li, J., 2015. Evaluation of water storage change of inland cryosphere in Northwestern China. Adv. Meteorol. 2015, 681634 https://doi.org/10.1155/2015/681634.

Yang, D., Shao, W., Yeh, P.J.F., Yang, H., Kanae, S., Oki, T., 2009. Impact of vegetation coverage on regional water balance in the nonhumid regions of China. Water Resour. Res. 45, W00A14. https://doi.org/10.1029/2008wr006948.

Yang, H., Qi, J., Xu, X., Yang, D., Lv, H., 2014. The regional variation in climate elasticity and climate contribution to runoff across China. J. Hydrol. 517, 607–616. https://doi.org/10.1016/j.jhydrol.2014.05.062.

Yang, Y., Roderick, M.L., Zhang, S., McVicar, T.R., Donohue, R.J., 2019. Hydrologic implications of vegetation response to elevated CO_2 in climate projections. Nat. Clim. Chang. 9 (1), 44–48. https://doi.org/10.1038/s41558-018-0361-0.

Yosef, G., Walko, R., Avisar, R., Tatarinov, F., Rotenberg, E., Yakir, D., 2018. Large-scale semi-arid afforestation can enhance precipitation and carbon sequestration potential. Sci. Rep. 8 (1), 996. https://doi.org/10.1038/s41598-018-19265-6.

Yu, L., Xue, Y., Diallo, I., 2021. Vegetation greening in China and its effect on summer regional climate. Sci. Bull. 66 (1), 13–17. https://doi.org/10.1016/j.scib.2020.09.003.

Yu, P., Wang, Y., Wu, X., Dong, X., Xiong, W., Bu, G., et al., 2010. Water yield reduction due to forestation in arid mountainous region, northwest China. J. Sediment Res. 25 (4), 426–433. https://doi.org/10.1016/S1001-6279(11)60009-7.

Yuan, W., Zheng, Y., Piao, S., Ciais, P., Lombardozzi, D., Wang, Y., et al., 2019. Increased atmospheric vapor pressure deficit reduces global vegetation growth. Sci. Adv. 5 (8), eaax1396. https://doi.org/10.1126/sciadv.aax1396.

Yurtseven, I., Serengil, Y., Gökbulak, F., Şengönül, K., Ozhan, S., Kılıç, U., et al., 2017. Results of a paired catchment analysis of forest thinning in Turkey in relation to forest management options. Sci. Total Environ. 618, 785–792. https://doi.org/10.1016/j.scitotenv.2017.08.190.

Zajac, Z., Revilla-Romero, B., Salamon, P., Burek, P., Hirpa, F.A., Beck, H., 2017. The impact of lake and reservoir parameterization on global streamflow simulation. J. Hydrol. 548, 552–568. https://doi.org/10.1016/j.jhydrol.2017.03.022.

Zeng, Z., Piao, S., Li, L.Z.X., Zhou, L., Ciais, P., Wang, T., et al., 2017. Climate mitigation from vegetation biophysical feedbacks during the past three decades. Nat. Clim. Chang. 7, 432–436. https://doi.org/10.1038/nclimate3299.

Zhai, R., Tao, F., 2021. Climate change in China affects runoff and terrestrial ecosystem water retention more than changes in leaf area index and land use/cover over the period 1982–2015. J. Geophys. Res. Biogeosci. 126, e2020JG005902 https://doi.org/10.1029/2020JG005902.

Zhao, F., Ma, S., Wu, Y., 2021. Changes in dry-season water availability and attributions in the Yellow River Basin, China. Front. Environ. Sci. 9, 762137 https://doi.org/10.3389/fenvs.2021.762137.

Zhang, D., Liu, X., Zhang, L., Zhang, Q., Gan, R., Li, X., 2020. Attribution of evapotranspiration changes in humid regions of China from 1982 to 2016. J. Geophys. Res. Atmos. 125, e2020JD032404 https://doi.org/10.1029/2020JD032404.

Zhang, H., Yu, J., Wang, P., Wang, T., Li, Y., 2021a. Groundwater-fed oasis in arid Northwest China: insights into hydrological and hydrochemical processes. J. Hydrol. 597, 126154 https://doi.org/10.1016/j.jhydrol.2021.126154.

Zhang, J., Zhang, Y., Sun, G., Song, C., Dannenberg, M.P., Li, J., et al., 2021b. Vegetation greening weakened the capacity of water supply to China's South-to-North water diversion project. Hydrol. Earth Syst. Sci. 25, 5623–5640. https://doi.org/10.5194/hess-25-5623-2021.

Zhang, L., Yu, G., Sun, X., Wen, X., Ren, C., Fu, Y., et al., 2006a. Seasonal variations of ecosystem apparent quantum yield (α) and maximum photosynthesis rate (Pmax) of

different forest ecosystems in China. Agric. For. Meteorol. 137, 176–187. https://doi.org/10.1016/j.agrformet.2006.02.006.

Zhang, S., Yang, Y., McVicar, T.R., Yang, D., 2018. An analytical solution for the impact of vegetation changes on hydrological partitioning within the Budyko framework. Water Resour. Res. 54, 519–537. https://doi.org/10.1002/2017WR022028.

Zhang, Y.Q., Kong, D.D., Zhang, X.Z., Tian, J., Li, C.C., 2021c. Impacts of vegetation changes on global evapotranspiration in the period 2003-2017. Acta Geogr. Sin. 76 (3), 584–594. https://doi.org/10.11821/dlxb202103007 in Chinese with English Abstract.

Zhang, Y.Q., Leuning, R., Chiew, F.H.S., Wang, E.L., Zhang, L., Liu, C.M., et al., 2012. Decadal trends in evaporation from global energy and water balances. J. Hydrometeorol. 13, 379–391. https://doi.org/10.1175/jhm-d-11-012.1.

Zhang, Y., Sha, L., Yu, G., Song, Q., Tang, J., Yang, X., et al., 2006b. Annual variation of carbon flux and impact factors in the tropical seasonal rain forest of Xishuangbanna, SW China. Sci. China Ser. D Earth Sci. 49 (S2), 150–162. https://doi.org/10.1007/s11430-006-8150-4.

Zhang, Z., Arnault, J., Wagner, S., Laux, P., Kunstmann, H., 2019. Impact of lateral terrestrial water flow on land-atmosphere interactions in the Heihe River Basin in China: fully coupled modeling and precipitation recycling analysis. J. Geophys. Res. Atmos. 124 (15), 8401–8423. https://doi.org/10.1029/2018JD030174.

Zhong, L., Ma, Y., Xue, Y., Piao, S., 2019. Climate change trends and impacts on vegetation greening over the Tibetan Plateau. J. Geophys. Res. Atmos. 124 (14), 7540–7552. https://doi.org/10.1029/2019JD030481.

Zhou, J., Wang, L., Zhang, Y., Guo, Y., Li, X., Liu, W., 2015. Exploring the water storage changes in the largest lake (Selin Co) over the Tibetan Plateau during 2003–2012 from a basin-wide hydrological modeling. Water Resour. Res. 51, 8060–8086. https://doi.org/10.1002/2014WR015846.

Zhou, S., Williams, A.P., Lintner, B.R., Berg, A.M., Zhang, Y., Keenan, T.F., et al., 2021. Soil moisture–atmosphere feedbacks mitigate declining water availability in drylands. Nat. Clim. Chang. 11, 38–44. https://doi.org/10.1038/s41558-020-00945-z.

Zhu, Z., Piao, S., Myneni, R.B., Huang, M., Zeng, Z., Canadell, J.G., et al., 2016. Greening of the earth and its drivers. Nat. Clim. Chang. 6 (8), 791–795. https://doi.org/10.1038/nclimate3004.

Zou, J., Zhan, C., Xie, Z., Qin, P., Jiang, S., 2016. Climatic impacts of the middle route of the south-to-north water transfer project over the Haihe River basin in North China simulated by a regional climate model. J. Geophys. Res. Atmos. 121 (15), 8983–8999. https://doi.org/10.1002/2016JD024997.